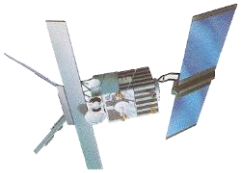
Spectral Representation in Oceanography: Observation and Modeling

Peter C. Chu
Naval Postgraduate School (NPS)

Collaborators:
Leonid Ivanov, Tatanya Margolina, C.W. Fan, Oleg Melnichenko, NPS
N.C. Wells, SOC, UK
Charles Sun, NOAA/NODC

Graduate Institute of Hydrological and Oceanic Sciences, National Central University, Taiwan, 29 December 2009.







How can we effectively use observational ocean data to represent and to model/predict the ocean state?







Outline

- (1) Theory and Methodology
- (2) Observational Application
  - ARGO Data: Baroclinic Rossby Waves in Tropical Atlantic
  - Surface Drifting Buoy Data: Synoptic Current Reversals on the Texas-Louisiana Continental Shelf
  - CODAR Data: Monterey Bay Surface Circulation
- (3) Modeling Application

Part-1
Theory and Methodology

References

- Chu, P.C., L.M. Ivanov, T.P. Korzhova, T.M. Margolina, and O.M. Melnichenko, 2003a: Analysis of sparse and noisy ocean current data using flow decomposition. Part 1: Theory. Journal of Atmospheric and Oceanic Technology, 20 (4), 478-491.

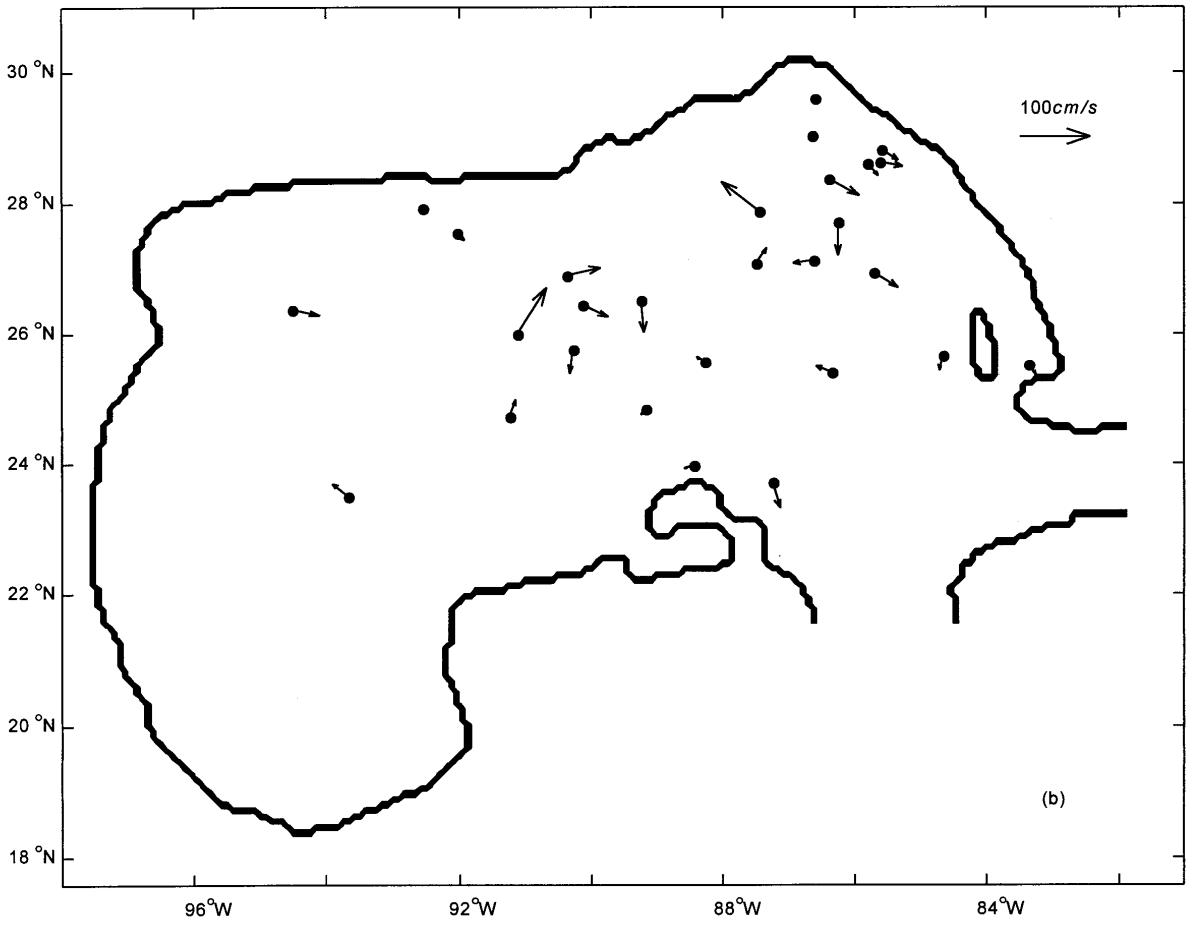
- Chu, P.C., L.M. Ivanov, T.P. Korzhova, T.M. Margolina, and O.M. Melnichenko, 2003b: Analysis of sparse and noisy ocean current data using flow decomposition. Part 2: Application to Eulerian and Lagrangian data. Journal of Atmospheric and Oceanic Technology, 20 (4), 492-512.

- Chu, P.C., L.M. Ivanov, and T.M. Margolina, 2004: Rotation method for reconstructing process and field from imperfect data. International Journal of Bifurcation and Chaos, 14(8), 2991-2997.

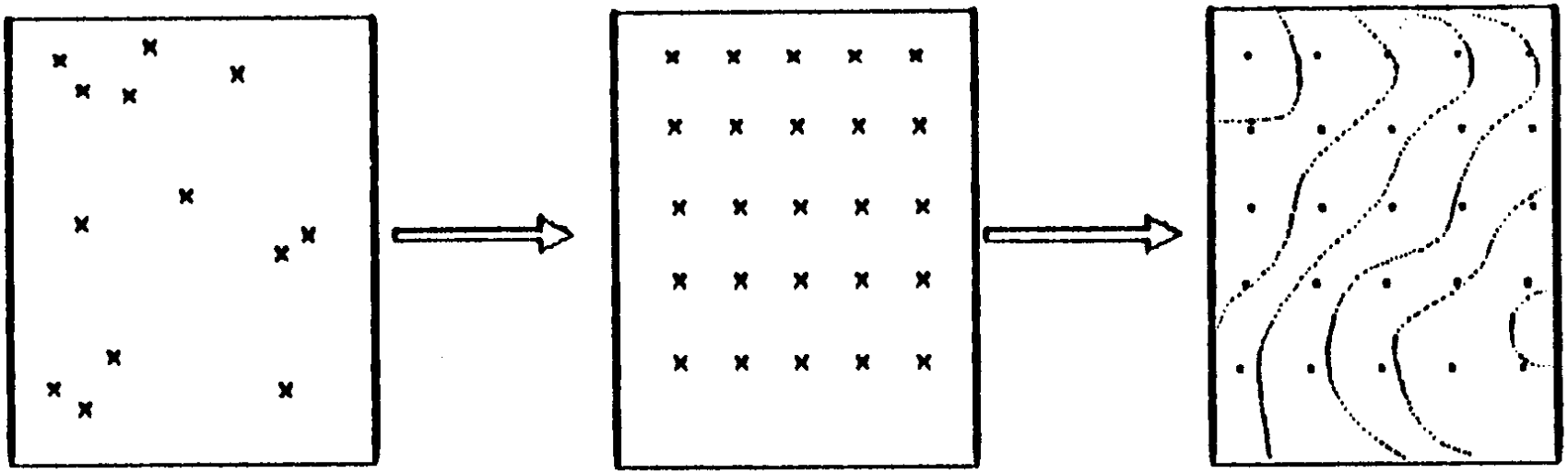
- These papers can be downloaded from:
- http://www.nps.edu/pcchu

Why do we need new data analysis and assimilation theory and methodology?

Observational Data (Sparse and Noisy)



Most Popular Method for Ocean Data Analysis: Optimum Interpolation (OI)



Three Necessary Conditions For the OI Method

- (1) First guess field
- (2) Autocorrelation functions
- (3) Low noise-to-signal ratio

Ocean velocity data

- (1) First guess field (?)
- (2) Unknown autocorrelation function
- (3) High noise-to-signal ratio

It is not likely to use the OI method to process ocean velocity data.

Major Methods of Ocean Data Assimilation

- Optimal Interpolation (OI) →

  Also a popular method for establishing gridded data such as (T, S) climate data, NODC/WOA, US-Russia EWG, …

- Kalman Filter

- Variational Methods

Static Instability

- Density inversion → Depth-decrease of density of two consecutive z-levels

→ Static instability

Less than 0.02 kg m^{-3} between the two consecutive levels is considered within the measurement errors of salinity (~ 0.02%) using the titration technique or measurement errors of temperature (~0.1^{o}C) (Levitus 1982).

Criterion of Density Inversion

$$\rho_k^a(n+1) - \rho_k^a(n) < -0.05 \text{ kg m}^{-3}$$

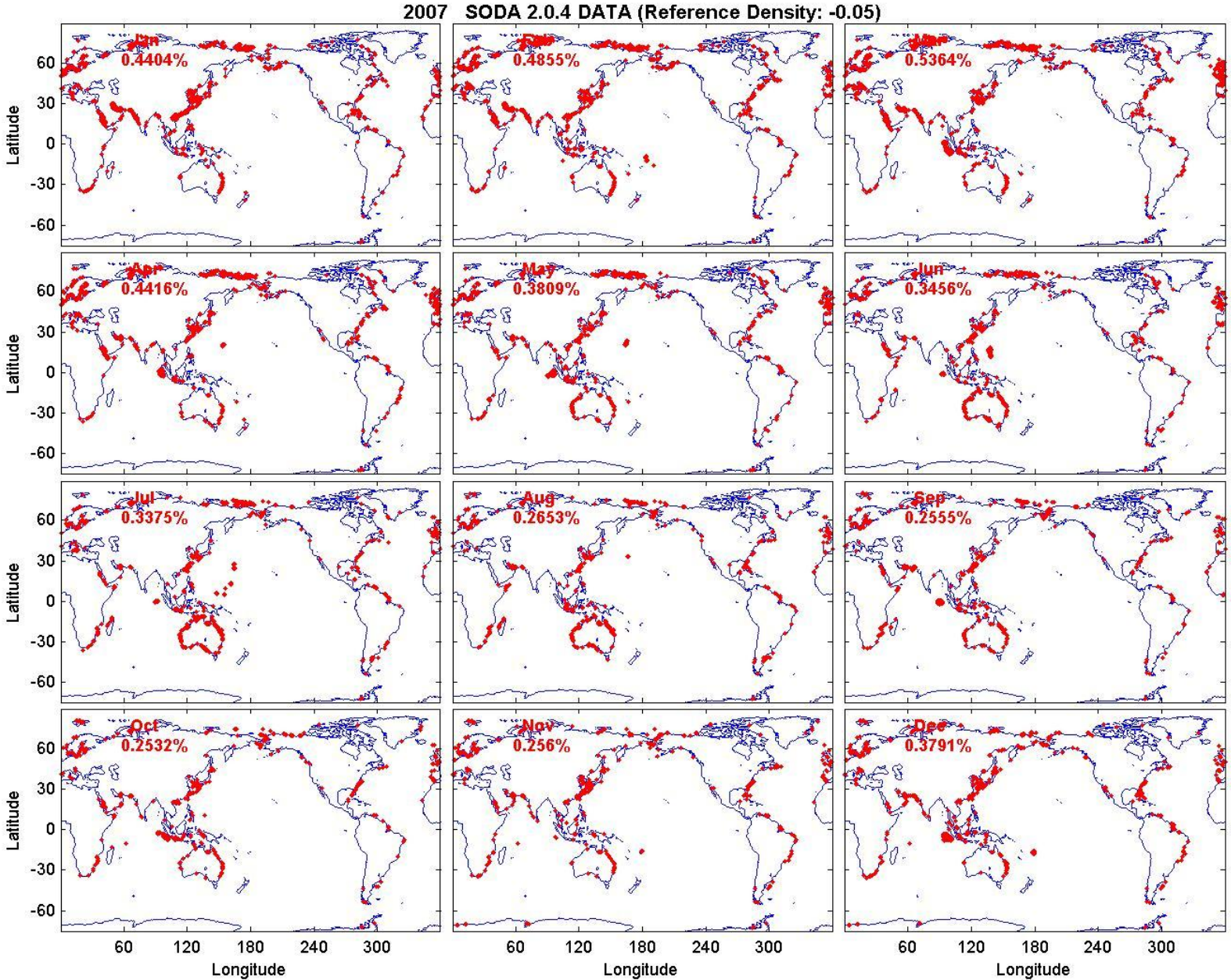
$n \rightarrow z$-level $\rightarrow z_n$

Here, n increases downward.

Example-1
Simple Ocean Data Assimilation (SODA)
Monthly

MOM-2b + OI

SODA 2007


2007 SODA 2.0.4 DATA (Reference Density: -0.05)
Jan
0.4404%
Feb
0.4855%
Mar
0.5364%
Apr
0.4416%
May
0.3809%
Jun
0.3456%
Jul
0.3375%
Aug
0.2653%
Sep
0.2555%
Oct
0.2532%
Nov
0.256%
Dec
0.3791%
Latitude
60
30
0
-30
-60
60
120
180
240
300
Longitude

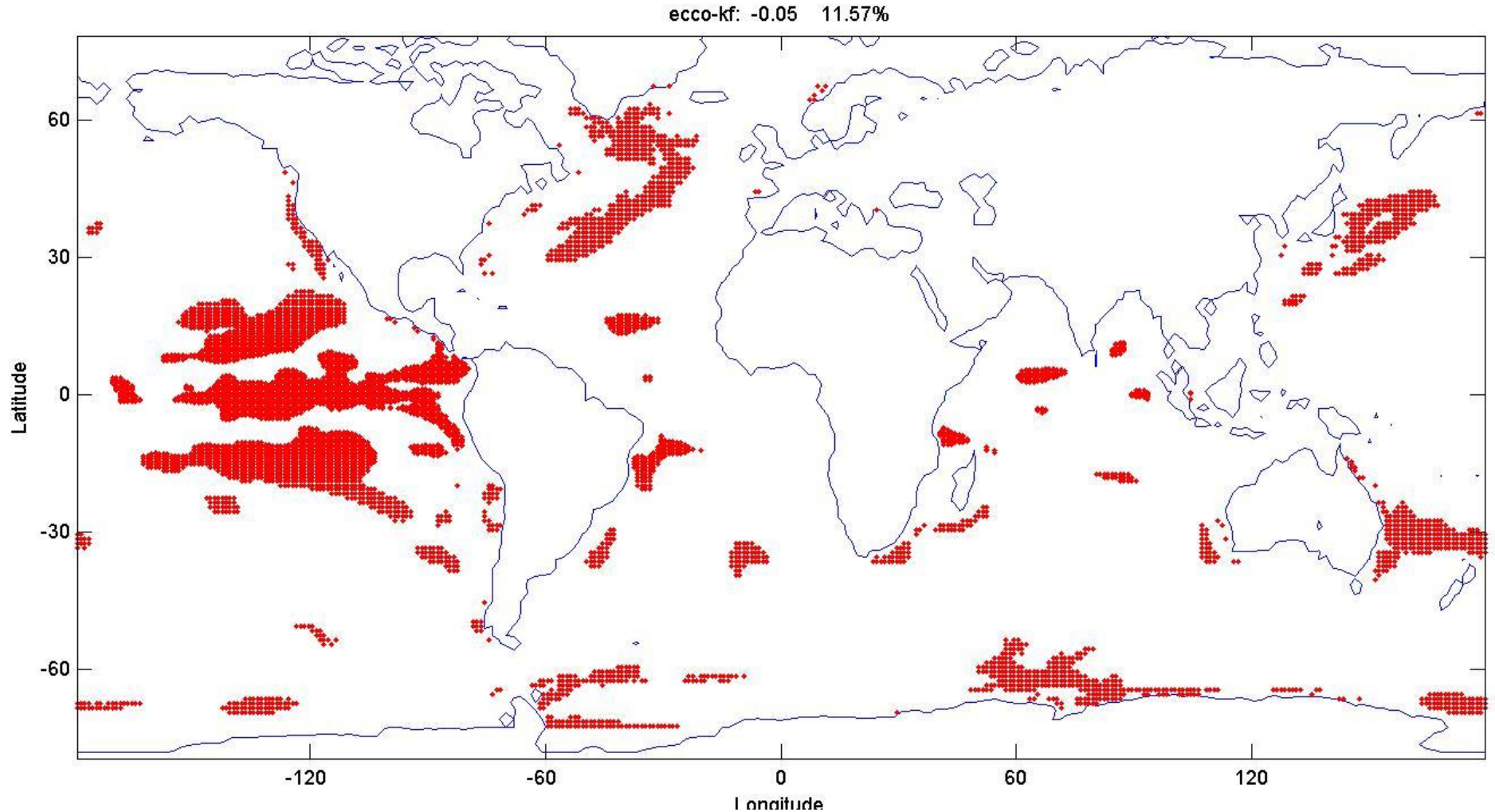
Example-2
JPL Estimating the Circulation and Climate of the Ocean (JPL-ECCO) 10 day

MIT General Circulation Model
+ Kalman Filter

JPL-ECCO 2007 (10-day)

Centered on Dec 31, 2008

Unstable Profiles → 11.57%

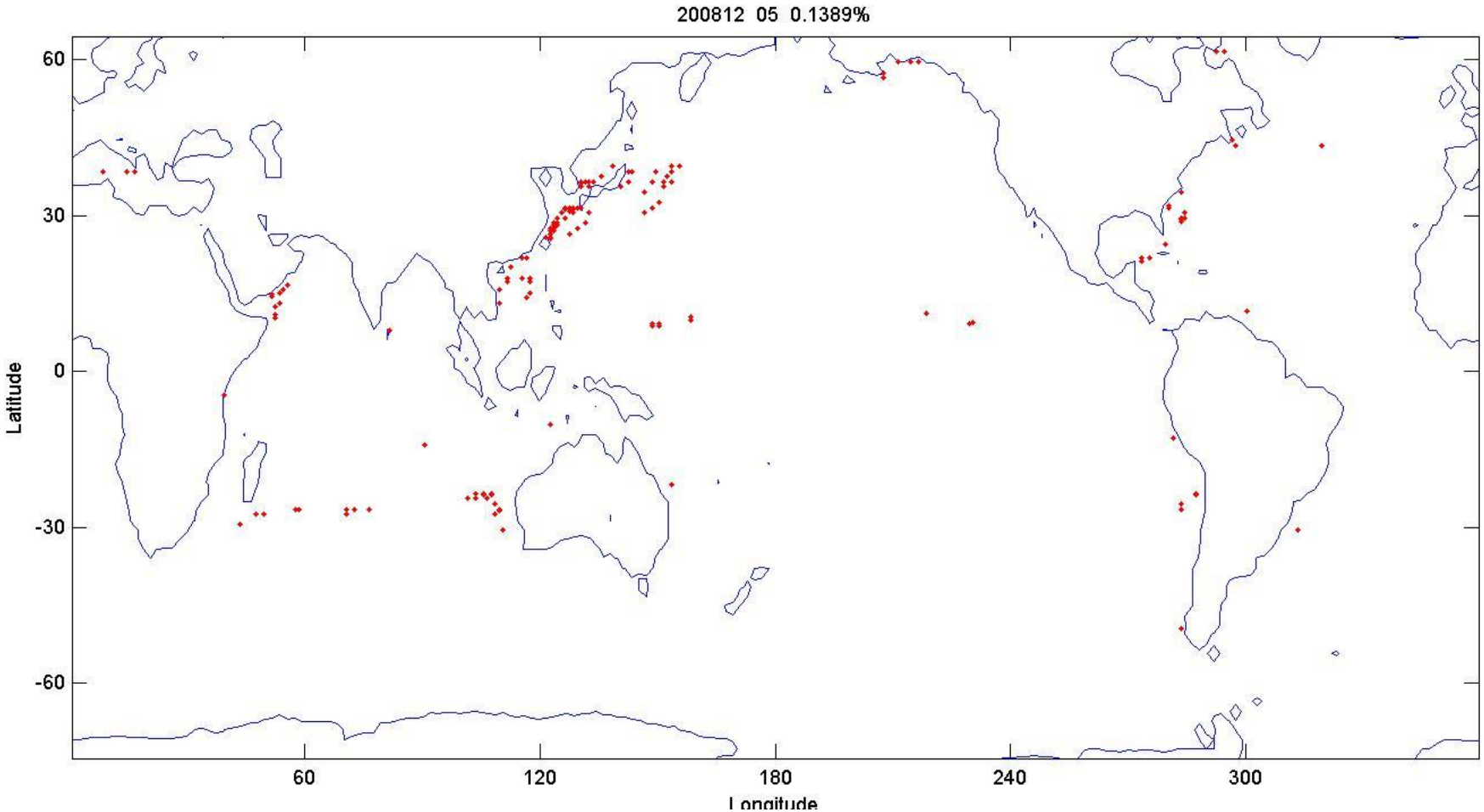


Example-3
NCEP Global Ocean Data Assimilation System (GODAS) Monthly

MOM + 3D-Var

GODAS December 2008

Unstable Profiles → 0.14%



Why?

- (1) The equation of the state of seawater is highly nonlinear.

$$\rho(S,T,p) = \frac{\rho(S,T,0)}{1 - p / K(S,T,p)}$$

- (2) Vertical structure of the (T, S) fields is not preserved during the data analysis/assimilation procedure conducted in the physical space (**i**, **j**, **k**).

Ocean Variables

$\mathbf{x}_t \rightarrow$ "true"

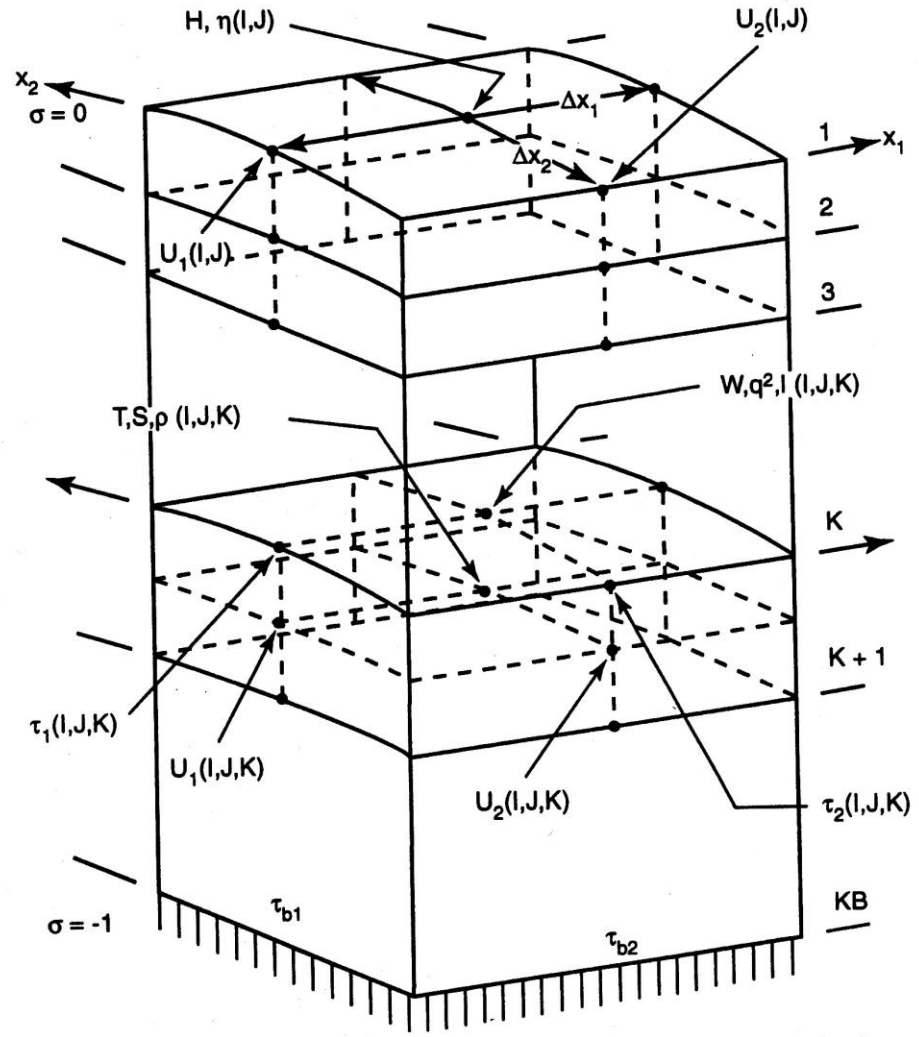
$\mathbf{x}_a \rightarrow$ analysis (model variables)

$\mathbf{x}_b \rightarrow$ background (or forecast)

$(\mathbf{x}_t, \mathbf{x}_a, \mathbf{x}_b) \rightarrow$ grid point (i)

$\mathbf{y}_o \rightarrow$ Observation $\rightarrow$ grid point (k)

Model Discretization



Spectral Representation - a Possible Alternative Method

Theoretical Base: Fourier Series Expansion

$$c(\mathbf{x}, z_k, t) = A_0(z_k, t) + \sum_{m=1}^{M} A_m(z_k, t)\ \Psi_m(\mathbf{x}, z_k),$$

Flow Decomposition

$$u = \frac{\partial \Psi}{\partial y} + \frac{\partial^2 \Phi}{\partial x \partial z}, \qquad v = -\frac{\partial \Psi}{\partial x} + \frac{\partial^2 \Phi}{\partial y \partial z},$$

- $$\triangle \Psi = -\zeta$$

$$\triangle \Phi = -w$$

Basis Functions (Closed Basin)

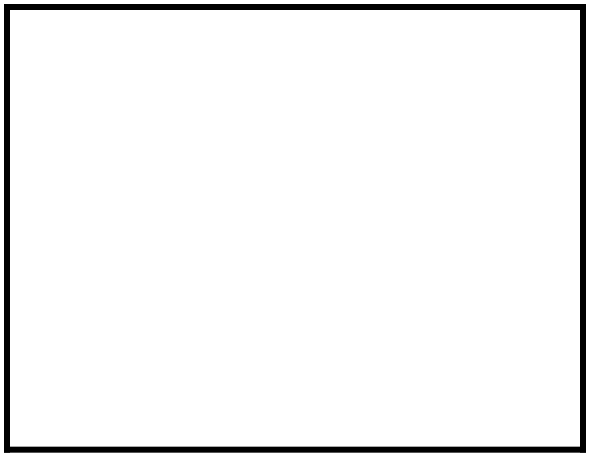
$$\triangle \Psi_k = -\lambda_k \Psi_k, \quad \Psi_k|_\Gamma = 0, \qquad k = 1, ..., \infty$$

$$\triangle \Phi_m = -\mu_m \Phi_m, \quad \frac{\partial \Phi_m}{\partial n}|_\Gamma = 0, \qquad m = 1, ..., \infty.$$

Eremeev et al. (1992 JGR)

Rectangular Domain with Flat Bottom

Sinusoidal Basis Functions

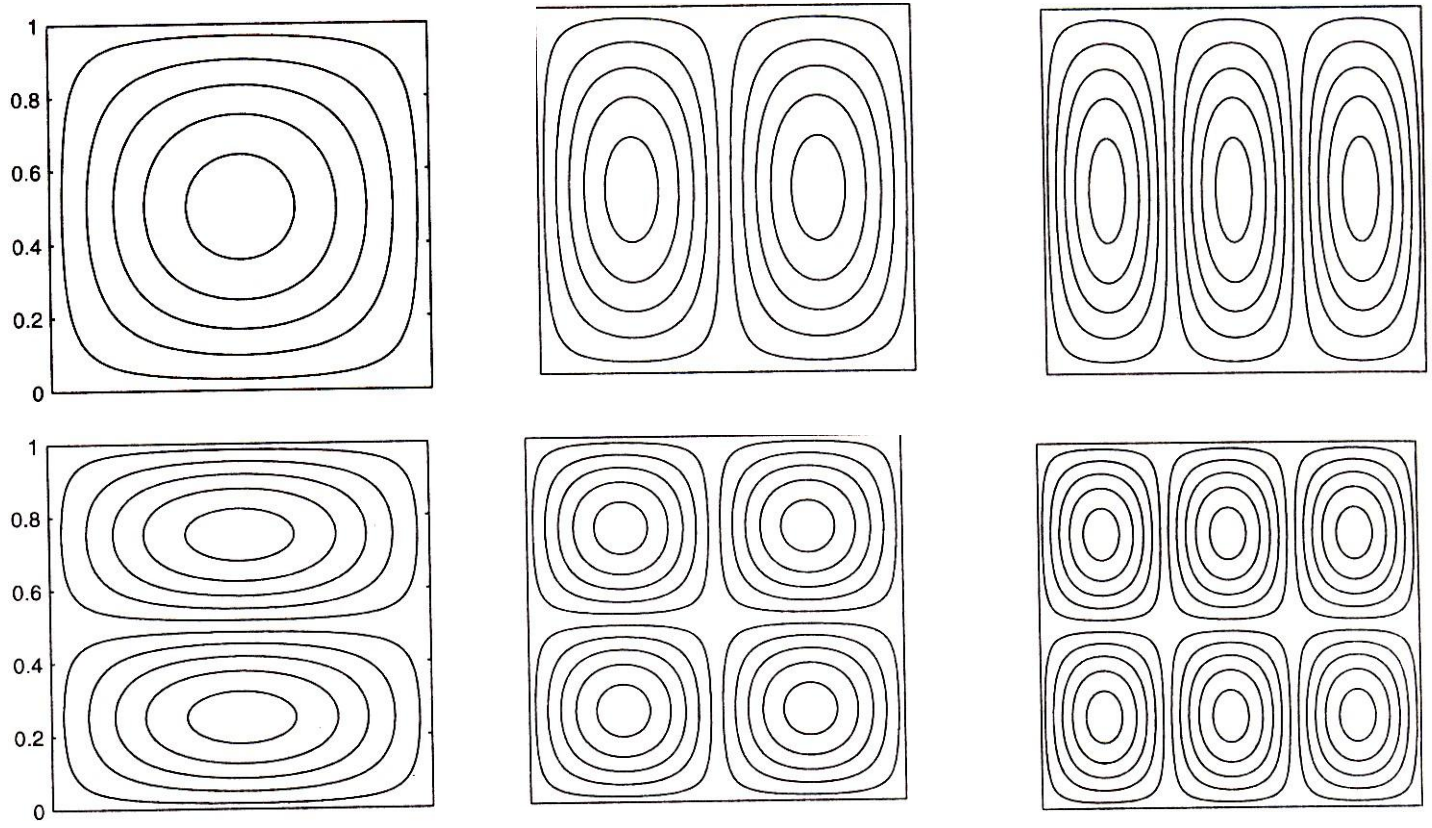


$$\Psi^{(i,j)} = \sin \frac{i\pi x}{L_x} \sin \frac{j\pi y}{L_y},$$

$$\Phi^{(i,j)} = \cos \frac{i\pi x}{L_x} \cos \frac{j\pi y}{L_y}$$

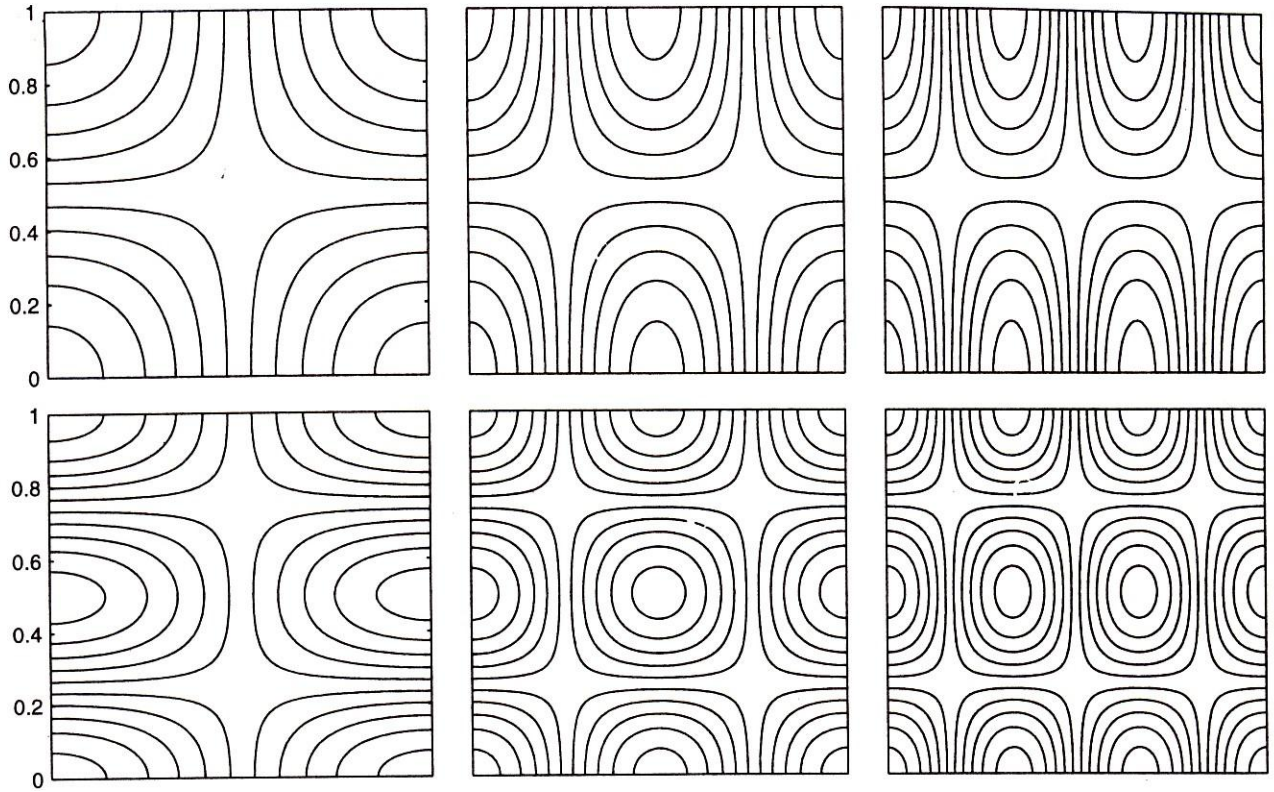
Basis Functions for Rectangular Domain

$$\Psi^{(i,j)} = \sin \frac{i\pi x}{L_x} \sin \frac{j\pi y}{L_y},$$



Basis Functions for Rectangular Domain

$$\Phi^{(i,j)} = \cos\frac{i\pi x}{L_x}\cos\frac{j\pi y}{L_y}$$



Basis Functions (Open Boundaries)

(Chu et al., 2003 a,b JTECH)

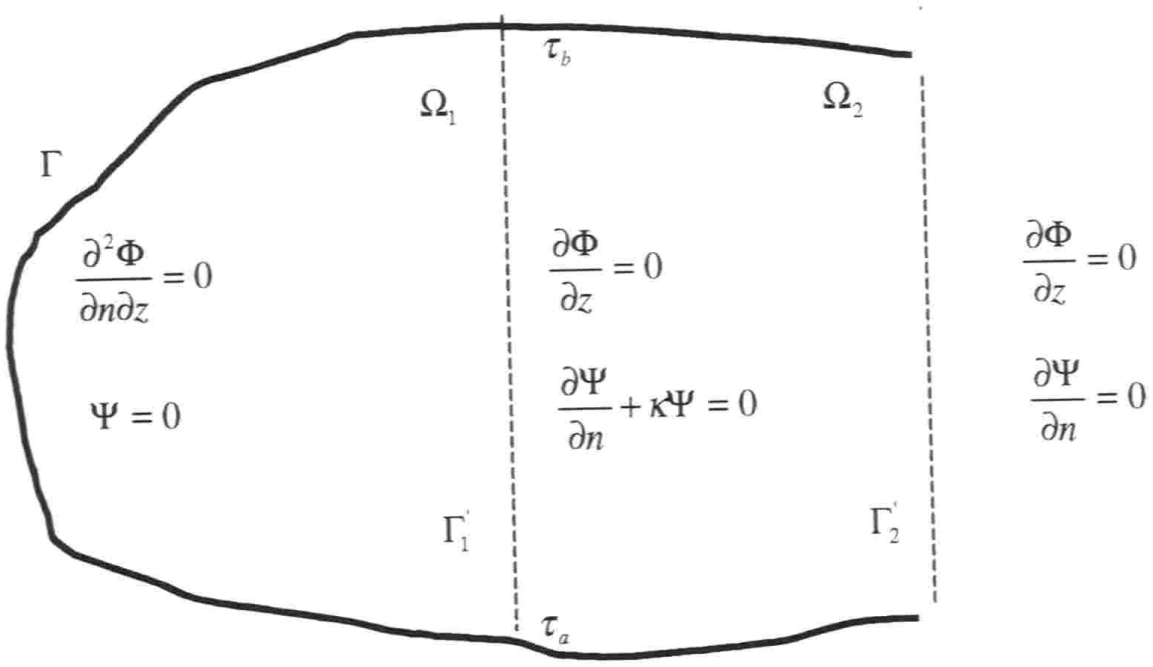
$$\triangle \Psi_k = -\lambda_k \Psi_k,$$

$$\triangle \Phi_m = -\mu_m \Phi_m,$$

$$\Psi_k|_\Gamma = 0, \quad \frac{\partial \Phi_m}{\partial n}|_\Gamma = 0,$$

$$\left[\frac{\partial \Psi_k}{\partial n} + \kappa(\tau)\Psi_k\right]|_{\Gamma_1'} = 0, \quad \Phi_m|_{\Gamma_1'} = 0,$$

Boundary Conditions



Spectral Decomposition

$$u_{KM} = \sum_{k=1}^{K} a_k(z,t^\circ)\frac{\partial \Psi_k(x,y,z,\kappa^\circ)}{\partial y} + \sum_{m=1}^{M} b_m(z,t^\circ)\frac{\partial \Phi_m(x,y,z)}{\partial x},$$

$$v_{KM} = -\sum_{k=1}^{K} a_k(z,t^\circ)\frac{\partial \Psi_k(x,y,z,\kappa^\circ)}{\partial x} + \sum_{m=1}^{M} b_m(z,t^\circ)\frac{\partial \Phi_m(x,y,z)}{\partial y}$$

Benefit of Using OSD

- Ocean Topographic Configuration →

  Basis Functions (Pre-Determined)

Optimal Mode Truncation

$$J(a_{1,\ldots,}a_K, b_{1,\ldots,}b_M, \kappa, P) = \frac{1}{2}\left(\left\|u_p^{obs} - u_{KM}\right\|_P^2 + \left\|v_p^{obs} - v_{KM}\right\|_P^2\right) \rightarrow \min,$$

Vapnik (1983) Cost Function →Optimal Mode Truncation

$$J_{emp} = J(a_{1,\ldots,}a_K, b_{1,\ldots,}b_M, \kappa, P).$$

$$\text{Prob}\left\{ \sup_{K,M,S} |\langle J(K,M,S)\rangle - J_{emp}(K,M,S)| \geq \mu \right\} \leq g(P,\mu)$$

$$\lim_{P\to\infty} g(P,\mu) = 0$$

Optimal Truncation

- Gulf of Mexico, Monterey Bay, Louisiana-Texas Shelf, Tropical Atlantic

- $K_{opt} = 40$, $M_{opt} = 30$

Determination of Spectral Coefficients (Ill-Posed Algebraic Equation)

$$\mathbf{A}\hat{\mathbf{a}} = \mathbf{QY},$$

Rotation Method (Chu et al., 2004)

$$\mathbf{SA}\,\hat{\mathbf{a}} = \mathbf{SQY},$$

$$J_1 = \|\mathbf{A}\|^2 - \frac{\|\mathbf{SQY}\|^2}{\|\mathbf{a}\|^2} \rightarrow \max,$$

Part-2
Observational Applications

(a) Baroclinic Rossby Waves in the tropical North Atlantic at mid-depth (ARGO)

(b) Synoptic Current Reversals on the Texas-Louisiana Continental Shelf (Surface Drifting Buoys)

(c) Monterey Bay Surface Circulation (CODAR)

(a) Baroclinic Rossby Waves in the tropical North Atlantic at mid-depth (ARGO)

References

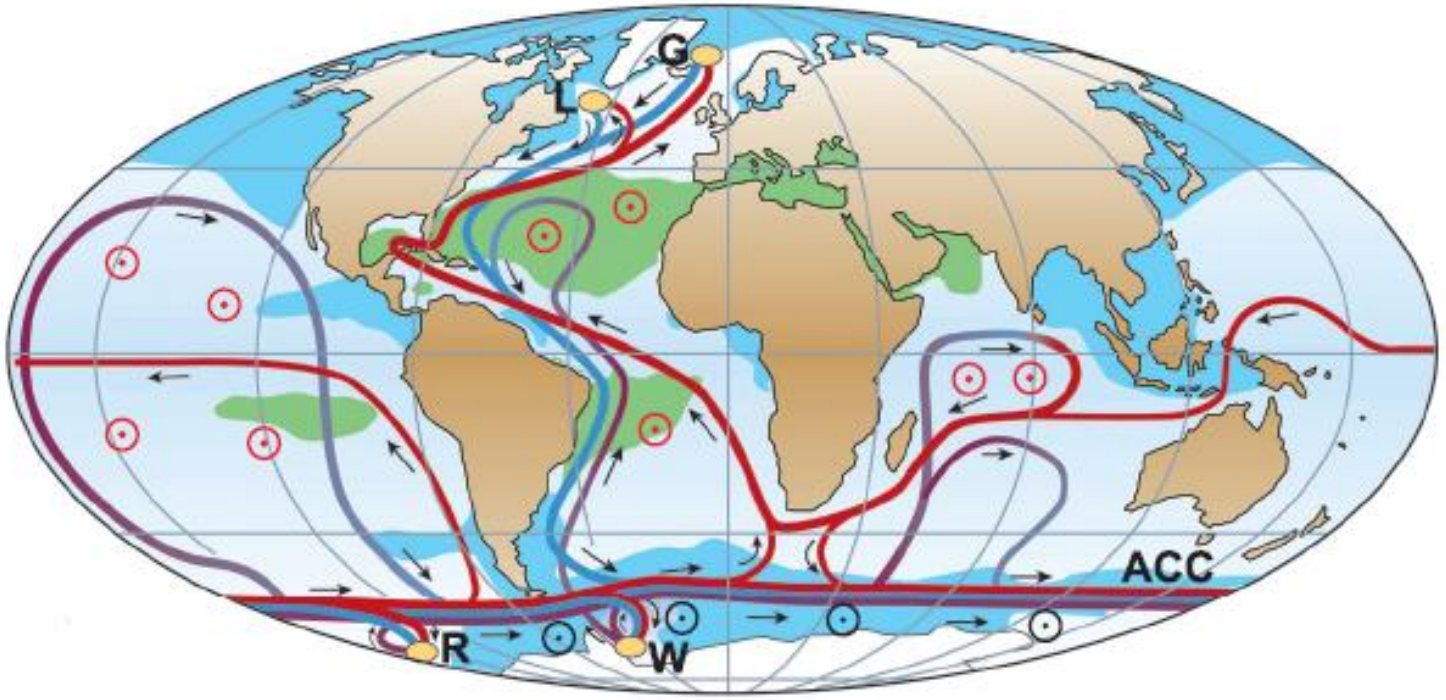
- Chu, P.C., L.M. Ivanov, and O.M. Melnichenko, 2005: Fall-winter current reversals on the Texas-Lousiana continental shelf. Journal of Physical Oceanography, 35, 902-910

- Chu, P.C., L.M. Ivanov, O.M. Melnichenko, and N.C. Wells, 2007: On long baroclinic Rossby Waves in the tropical North Atlantic observed from profiling floats. Journal of Geophysical Research – Oceans, 112, C05032, doi:10.1029/2006JC003698.

- These papers can be downloaded from:
- http://www.nps.edu/pcchu

Tropical North Atlantic (4° -24°N)
Important Transition Zone →
Meridional Overturning Circulation (MOC)

(Rahmstorf 2006)



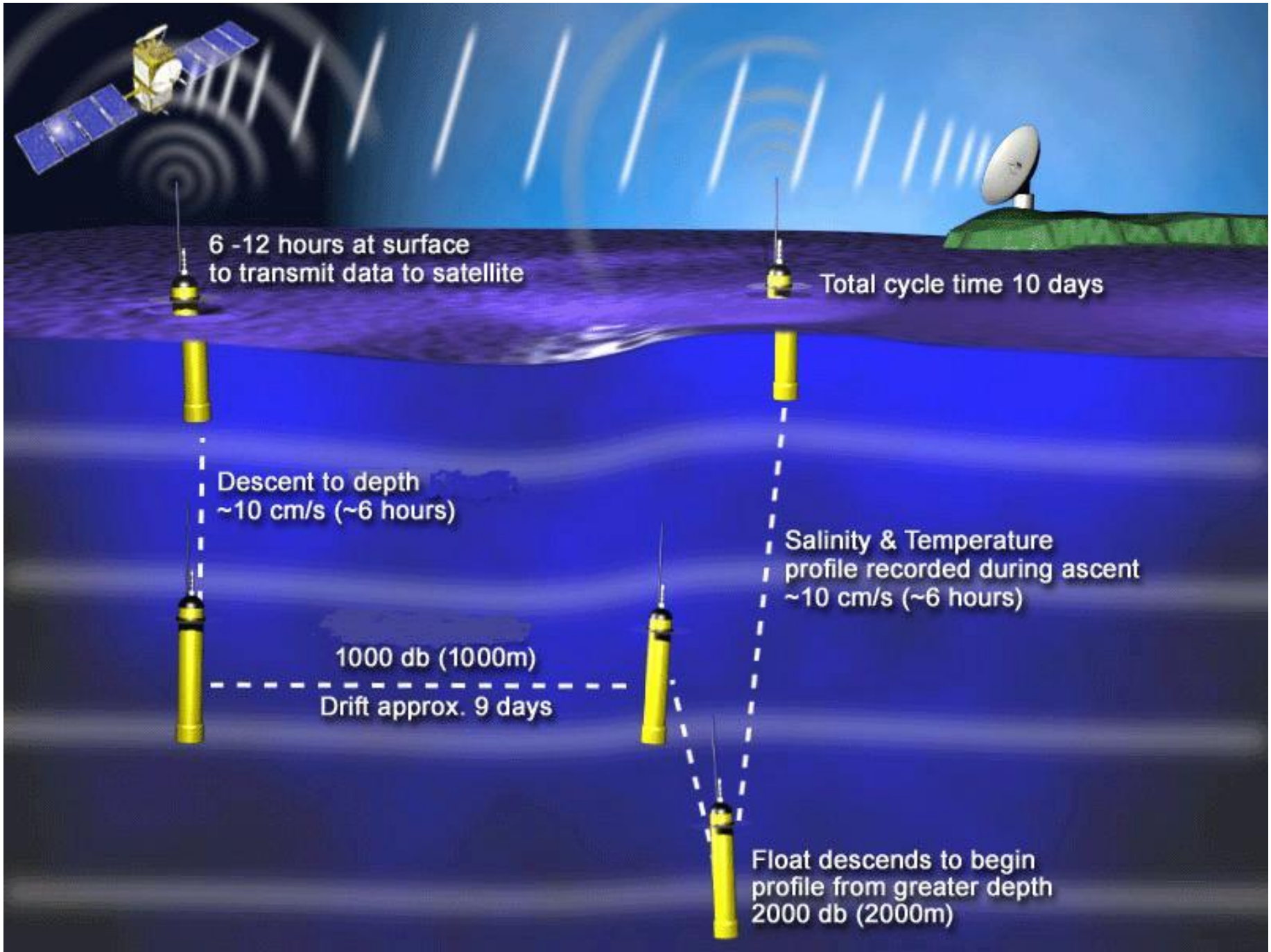
MOC Variation →

Heat Transport Variation →

Climate Change

- Are mid-depth (~1000 m) ocean circulations steady?

- If not, what mechanisms cause the change? (Rossby wave propagation)


6 -12 hours at surface
to transmit data to satellite
Total cycle time 10 days
Descent to depth
~10 cm/s (~6 hours)
Salinity & Temperature
profile recorded during ascent
~10 cm/s (~6 hours)
1000 db (1000m)
Drift approx. 9 days
Float descends to begin
profile from greater depth
2000 db (2000m)

Monthly Temperature (10 m) in the Pacific Ocean since 1990 (analyzed from GTSPP)



Monthly Temperature (200 m) in the Pacific Ocean since 1990



Monthly Temperature (500 m) in the Pacific Ocean since 1990



Monthly Temperature (1000 m) in the Pacific Ocean since 1990



Monthly Temperature (10 m) in the Atlantic Ocean since 1990



Monthly Temperature (200 m) in the Atlantic Ocean since 1990



Monthly Temperature (500 m) in the Atlantic Ocean since 1990



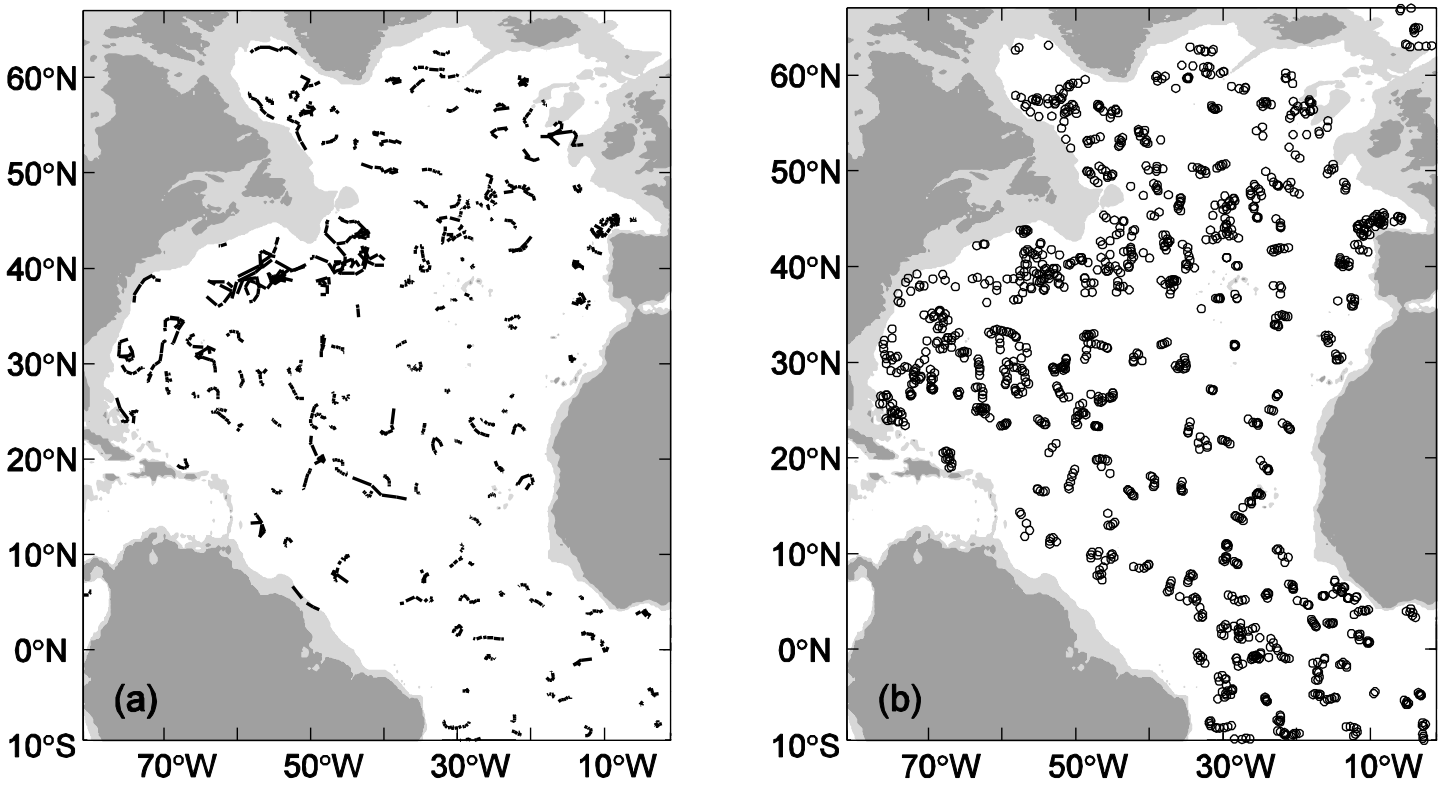
Monthly Temperature (1000 m) in the Atlantic Ocean since 1990



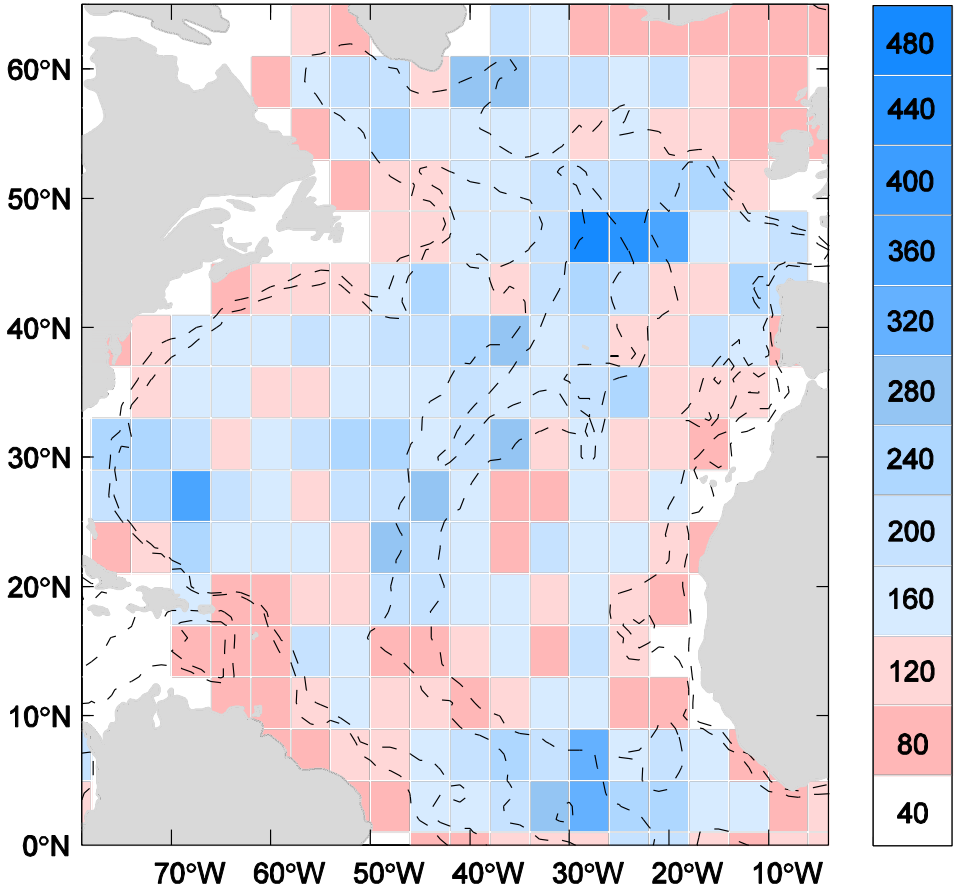
ARGO Observations (Oct-Nov 2004)

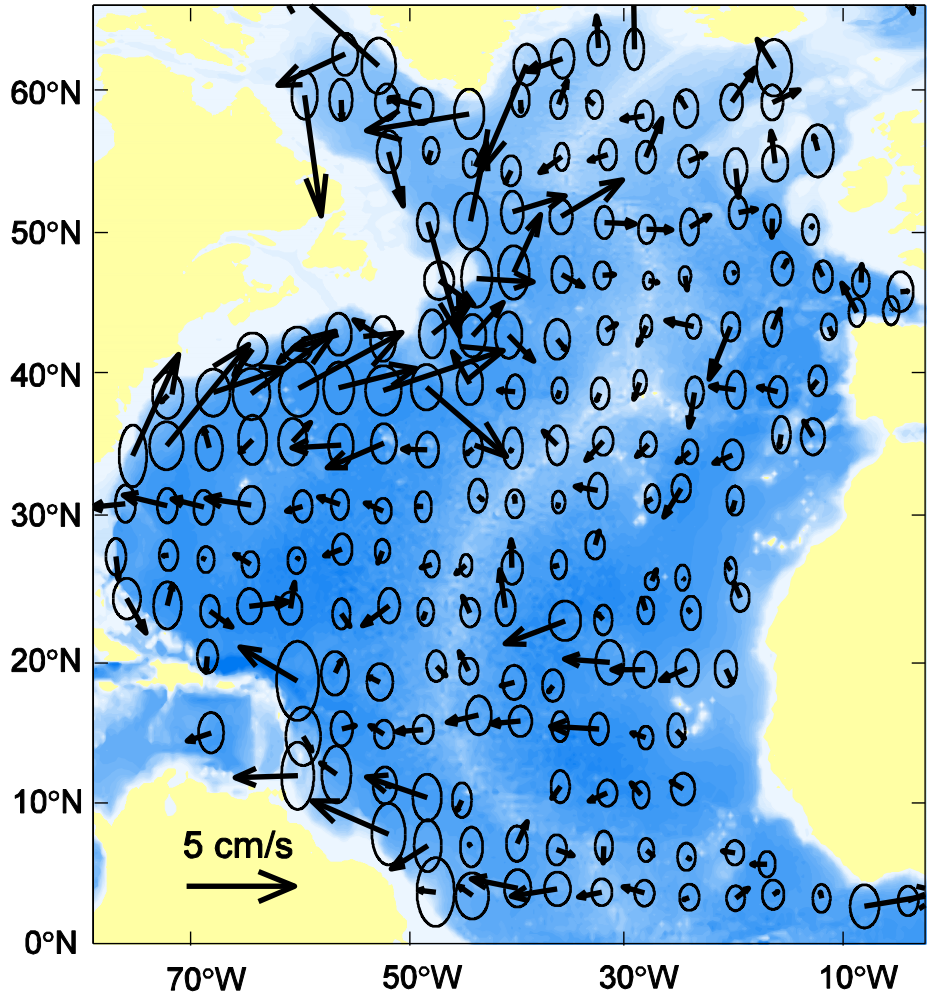
(a) Subsurface tracks

(b) Float positions where (T,S) were measured



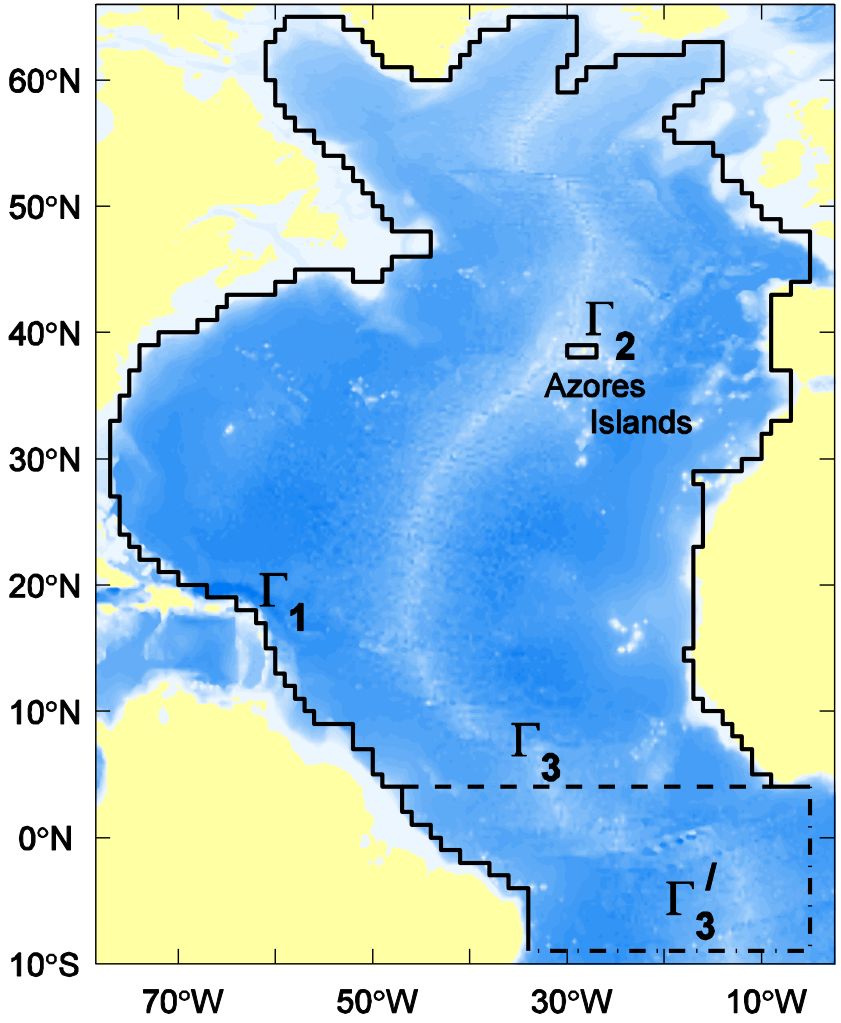
Circulations at 1000 m estimated from the original ARGO float tracks (bin method)
April 2004 – April 2005



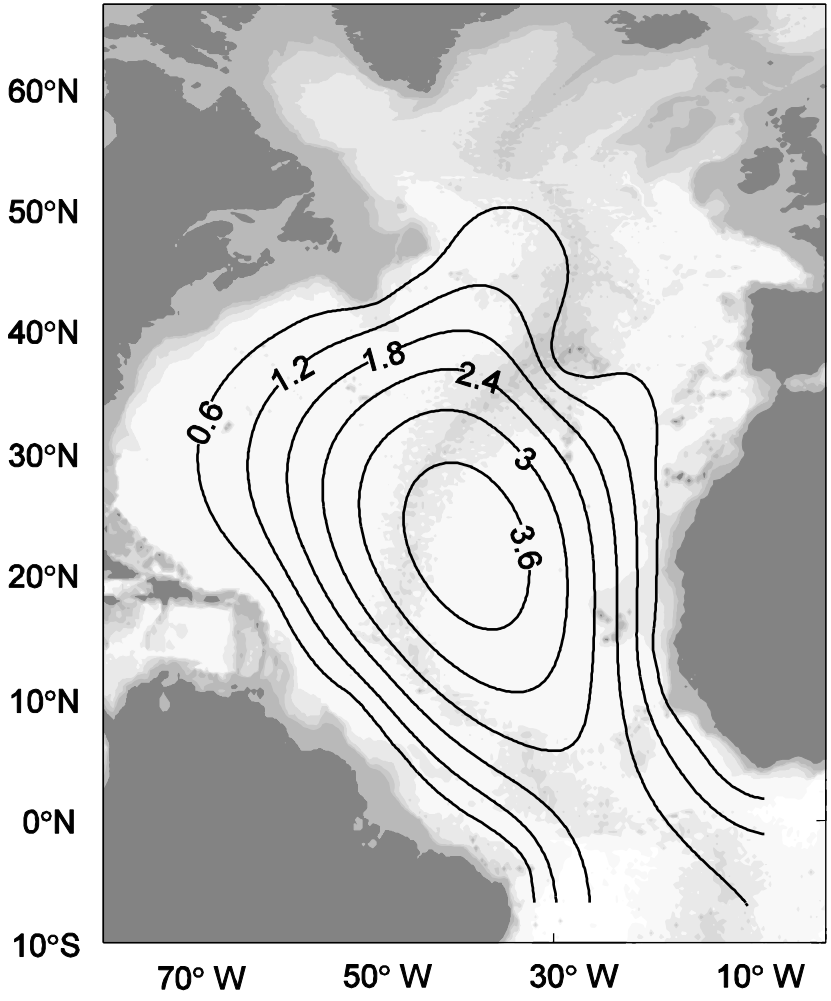


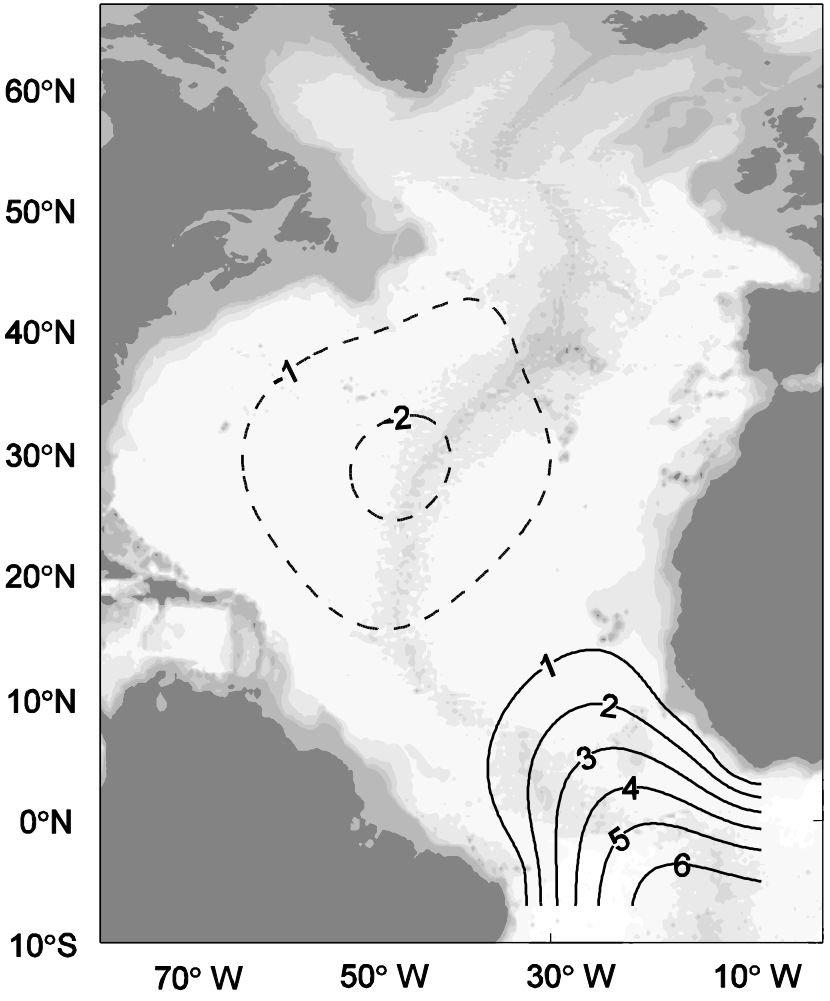
It is difficult to use such noisy data into ocean numerical models.

Boundary Configuration → Basis Functions for OSD



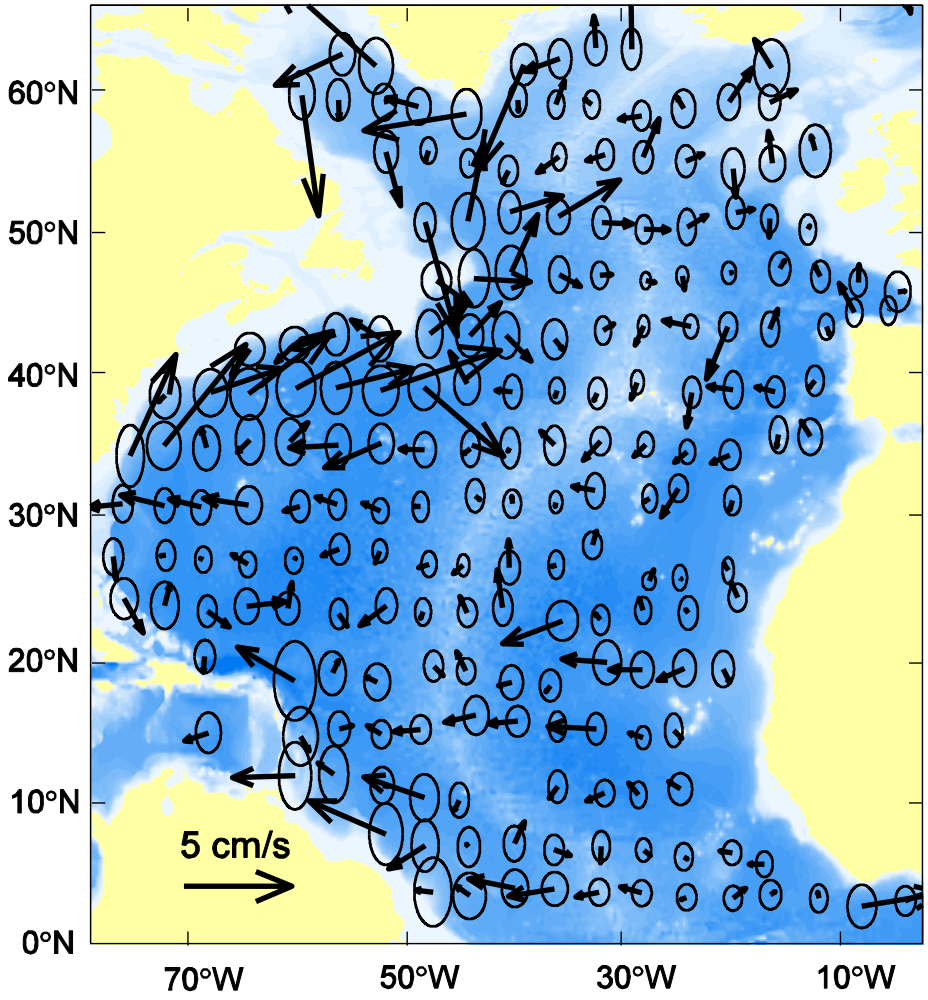
Basis Functions for Streamfunction Mode-1 and Mode-2



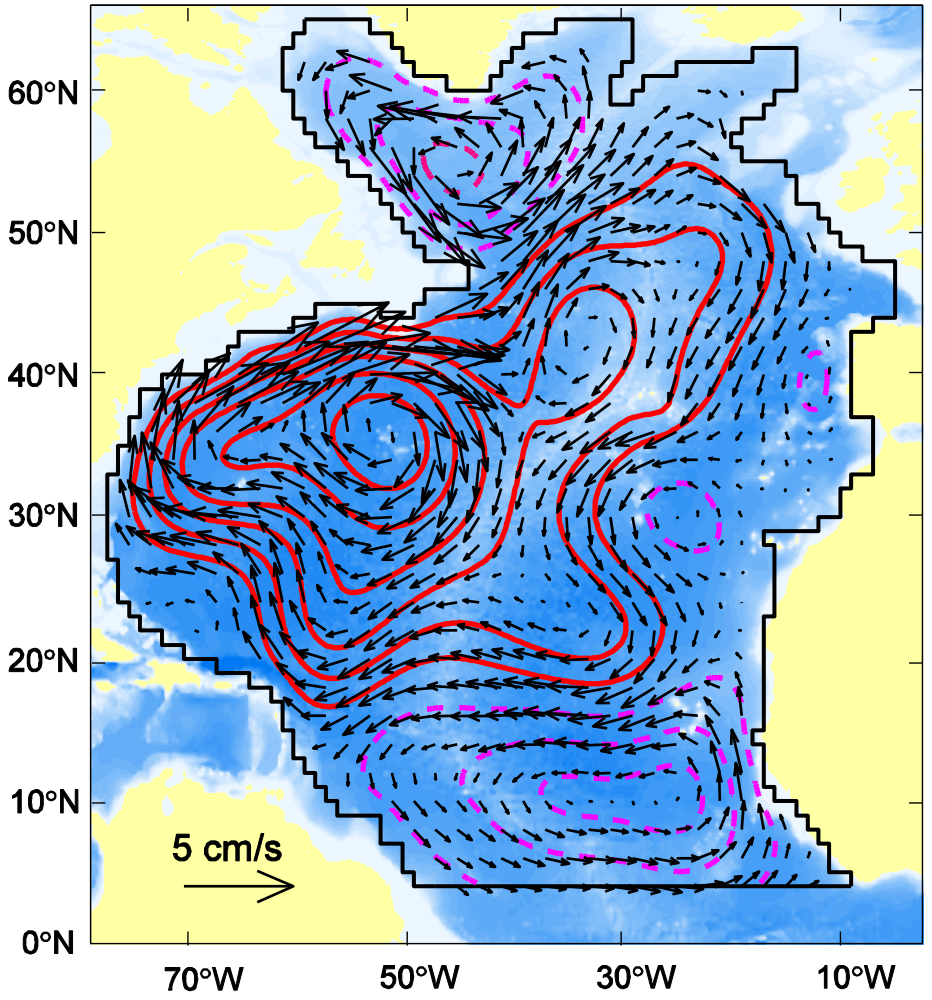


Circulations at 1000 m (March 04 to May 05)

Bin Method



OSD



Fourier Expansion → Temporal Annual and Semi-anuual

$$\hat{\psi} \approx \overline{\psi}(\mathbf{x}_\perp) + \psi_1(\mathbf{x}_\perp, t) + \psi_2(\mathbf{x}_\perp, t),$$

$$\psi_1(\mathbf{x}_\perp, t) = \sum_{s=1}^{2} A_{\omega_1, s} \cos(\omega_1 t + \theta_{\omega_1, s}) Z_s(\mathbf{x}_\perp) + \sum_{k=1}^{K_{opt}} B_{\omega_1, k} \cos(\omega_1 t + \vartheta_{\omega_1, k}) \Psi_k(\mathbf{x}_\perp),$$

$$\psi_2(\mathbf{x}_\perp, t) = \sum_{s=1}^{2} A_{\omega_2, s} \cos(\omega_2 t + \theta_{\omega_2, s}) Z_s(\mathbf{x}_\perp) + \sum_{k=1}^{K_{opt}} B_{\omega_2, k} \cos(\omega_2 t + \vartheta_{\omega_2, k}) \Psi_k(\mathbf{x}_\perp),$$

T_0=12 months; $\omega_1 = 2\pi / T_0$; $\omega_2 = 4\pi / T_0$

Fourier Expansion → Temporal Annual and Semi-anuual

$$\hat{T}(\mathbf{x}_\perp, z, t) \approx \overline{T}(\mathbf{x}_\perp, z) + T_1(\mathbf{x}_\perp, z, t) + T_2(\mathbf{x}_\perp, z, t),$$

$$T_1(\mathbf{x}_\perp, z, t) = \sum_{m=1}^{M_{opt}} C_{\omega_1, m}(z) \cos[\omega_1 t + \chi_{\omega_1, m}(z)] \Xi_m(\mathbf{x}_\perp, z),$$

$$T_2(\mathbf{x}_\perp, z, t) = \sum_{m=1}^{M_{opt}} C_{\omega_2, m}(z) \cos[\omega_2 t + \chi_{\omega_{21}, m}(z)] \Xi_m(\mathbf{x}_\perp, z),$$

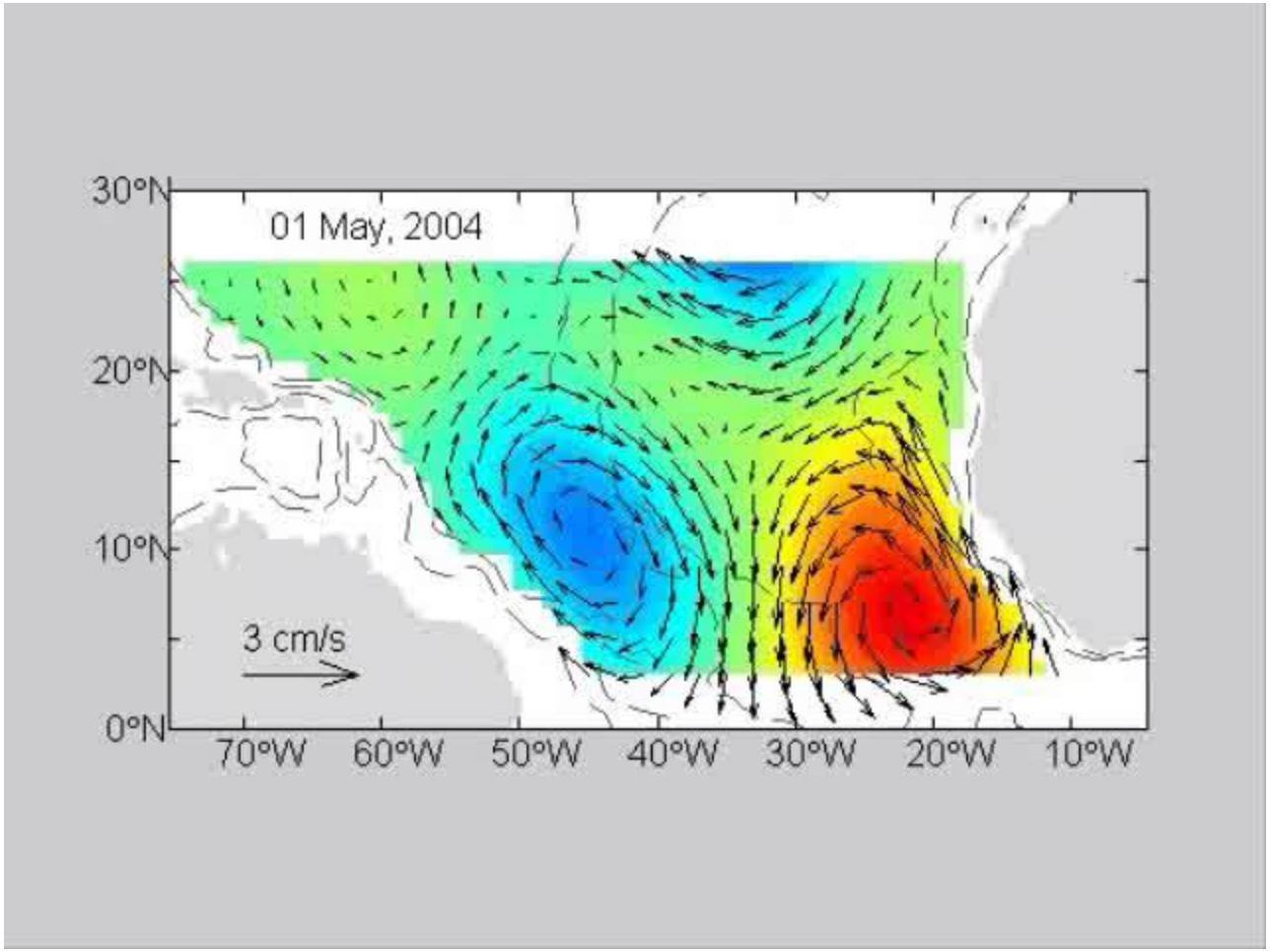
T_0=12 months; $\omega_1 = 2\pi / T_0$; $\omega_2 = 4\pi / T_0$

Optimization

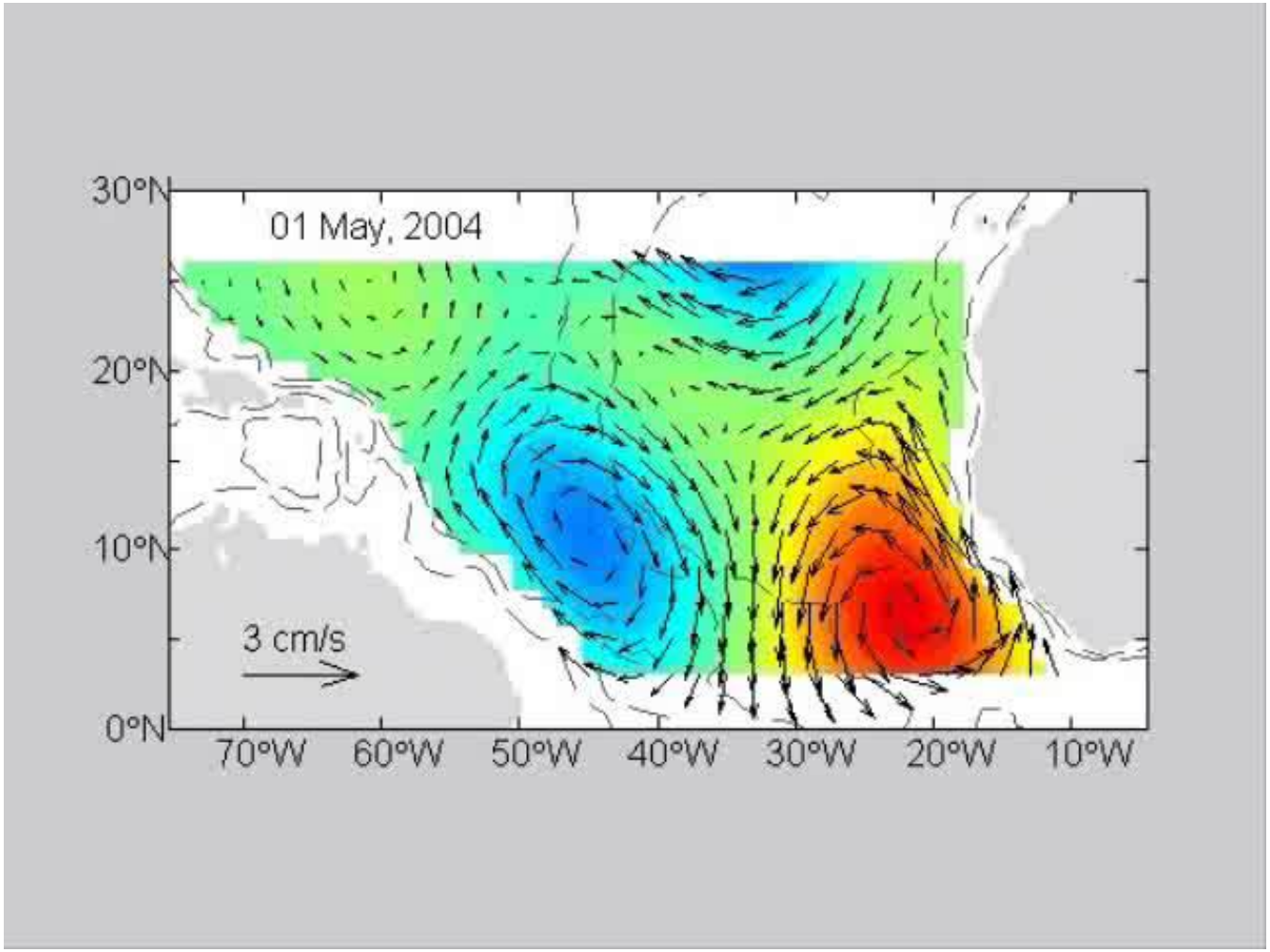
$$J_s = \int_{t_o}^{t_o+T_o} \left[a_s(t) - \sum_{\omega=\omega_1,\omega_2} A_{\omega,s} \cos(\omega t + \theta_{\omega,s}) \right]^2 dt \rightarrow \min$$

$$I_k = \int_{t_o}^{t_o+T_o} \left[b_k(t) - \sum_{\omega=\omega_1,\omega_2} B_{\omega,s} \cos(\omega t + \vartheta_{\omega,s}) \right]^2 dt \rightarrow \min$$

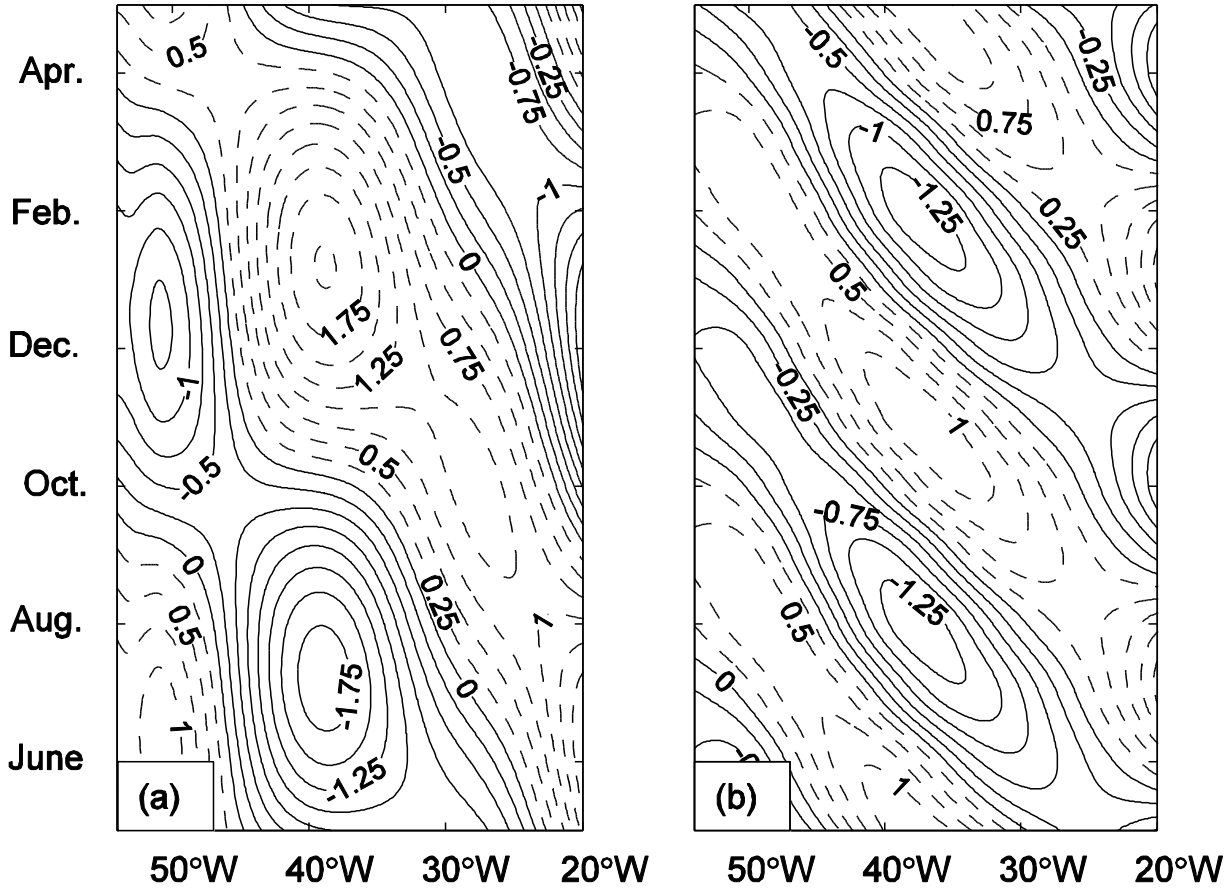
Annual Component



Semi-annual Component



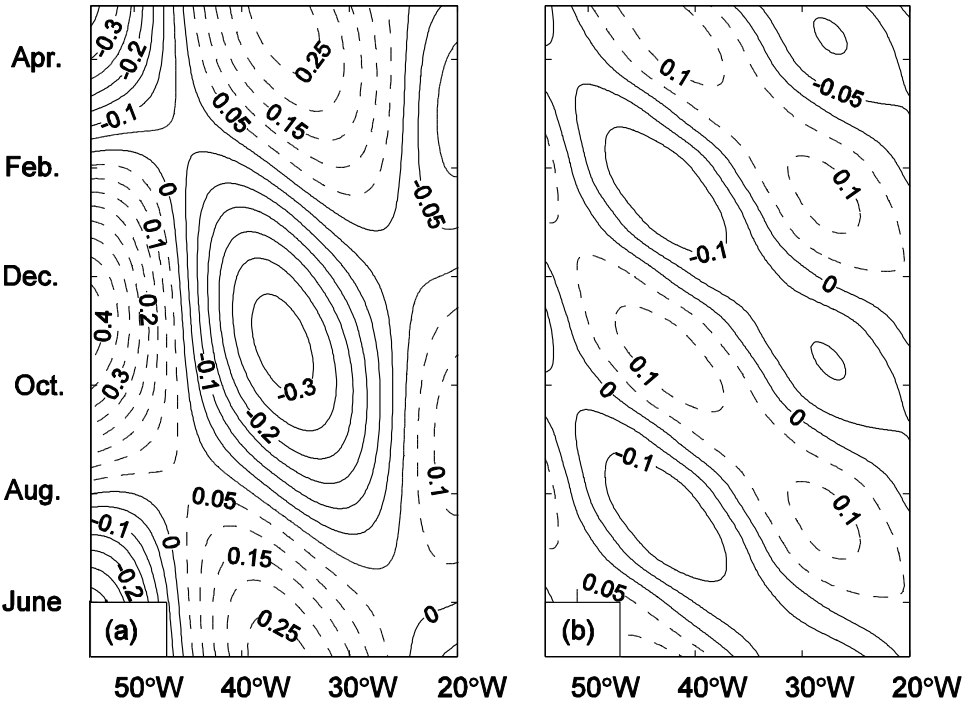
Time –Longitude Diagrams of Meridional Velocity Along 11°N



Annual

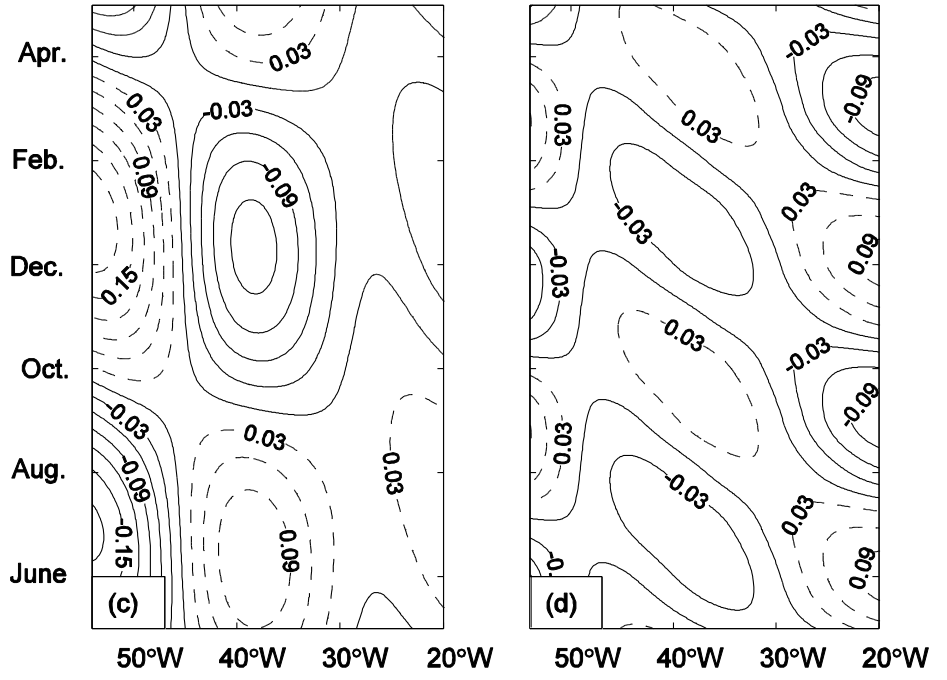
Semi-Annual

Time –Longitude Diagrams of temperature Along 11°N



Annual

Semi-Annual



Annual

Semi-Annual

550 m

950 m

Characteristics of Annual Rossby Waves

	March, 04 – May, 05 float data			March, 04 – May, 06 float data		
Latitude	c_p (cm/s)	L_1 (km)	L_2 (km)	c_p (cm/s)	L_1 (km)	L_2 (km)
5^0N	12	1200	1100	12	1300	900
8^0N	16	2500	1400	12	2100	1100
11^0N	14	2200	1400	11	1900	1100
13^0N	11	2100	1500	10	2300	1500

Western Basin

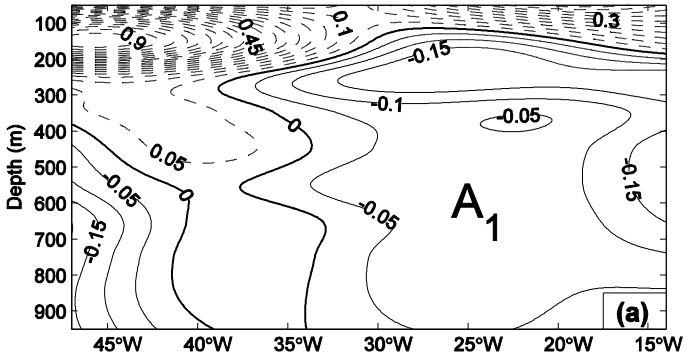
Eastern Basin

Western Basin

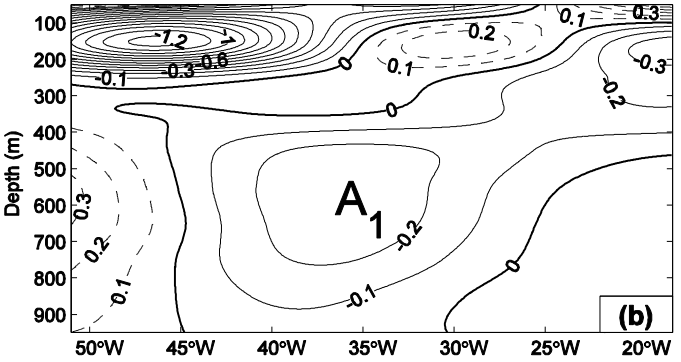
Eastern Basin

Zonal cross-sections of the annual component of the temperature anomaly (°C)

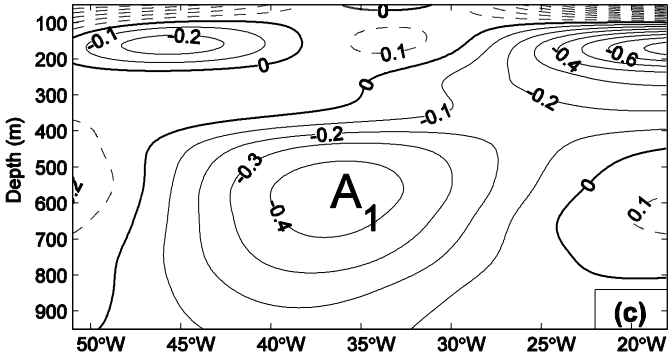
6°N in Jun 04 →



11°N in Oct, 04 →



16°N in Oct 04 →



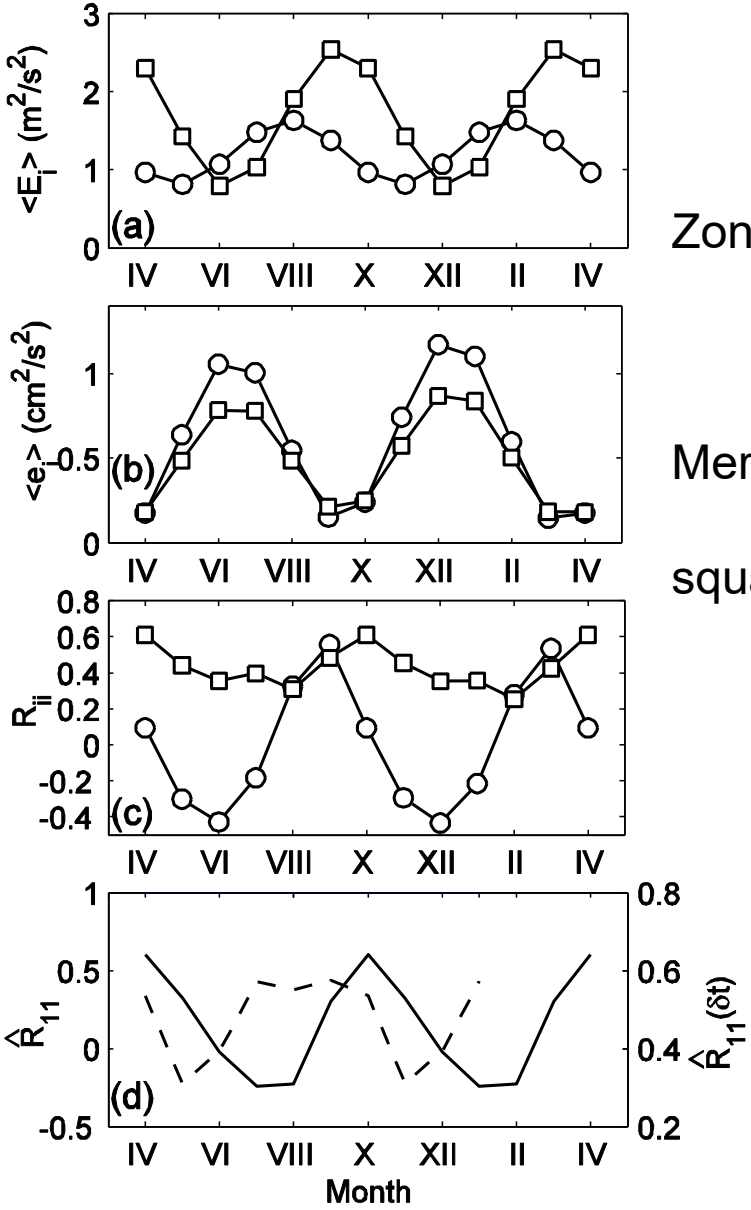
Annual Component in the Western Sub-Basin

Mean wind KE

Mean KE for mid-depth currents

Correlation between Winds and currents

Correlation between wind Stress curl and streamfunction (solid: no-lag, dashed: 3 mon lag



Zonal: circle

Meridional : square

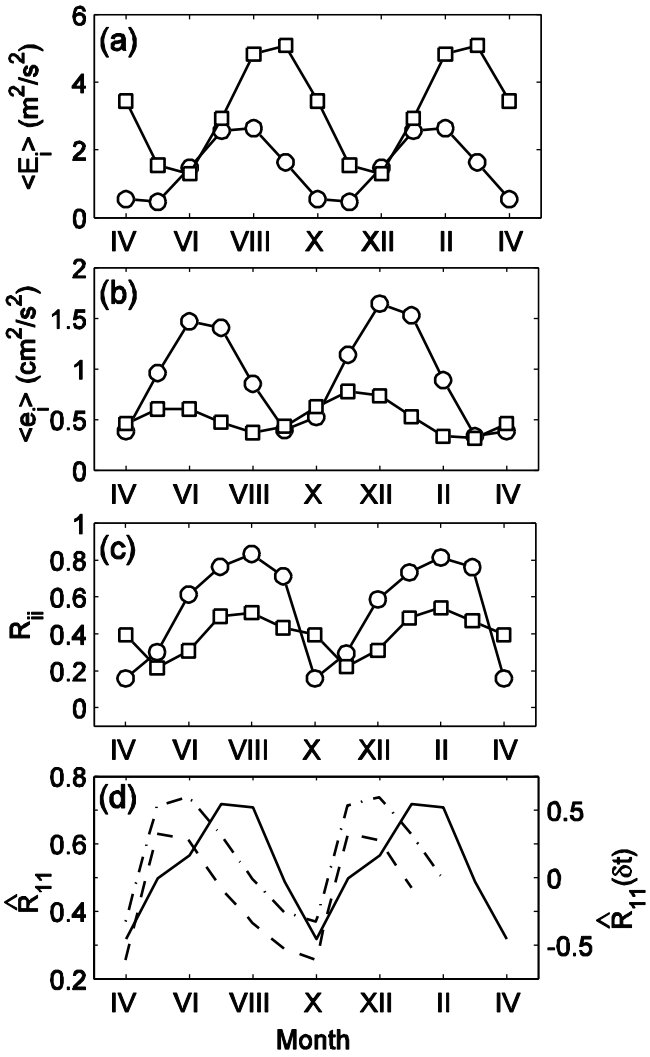
Annual Component in the Eastern Sub-Basin

Mean wind KE

Mean KE for mid-depth currents

Correlation between Winds and currents

Correlation between wind Stress curl and streamfunction (solid: no-lag, dashed: 3 mon lag



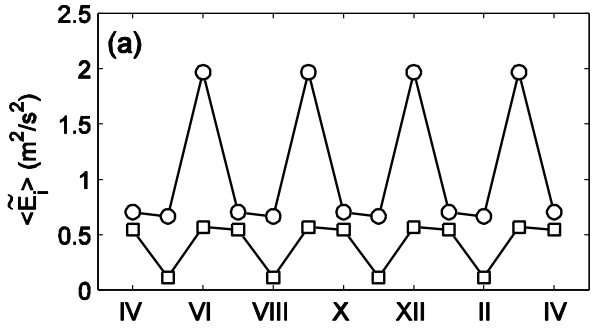
Zonal: circle

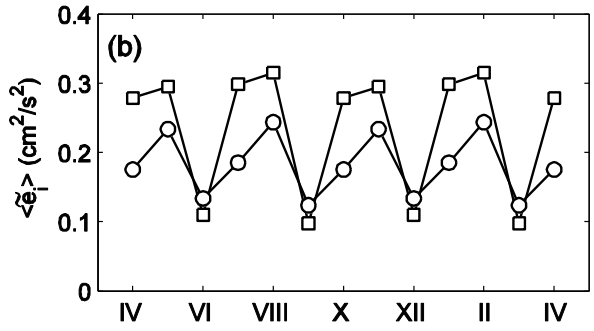
Meridional :

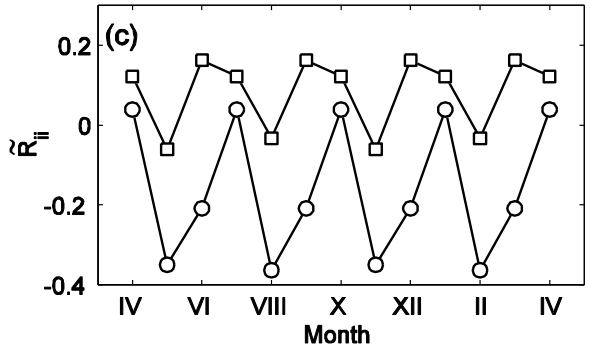
square

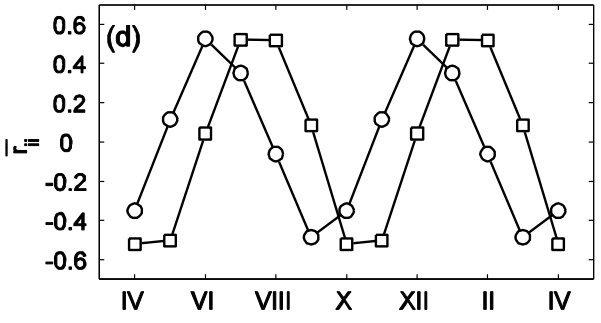
Semiannual Component in the Western Sub-Basin

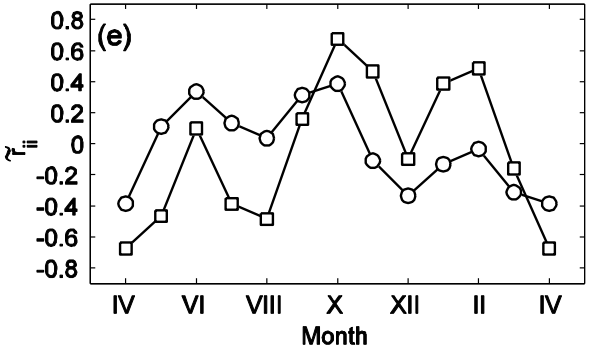
(a) wind KE
(b) current KE
(c) corr wind stress and currents
(d) corr between semi-annual currents and mean wind
(e) corr between semiannual currents and annual wind stress.





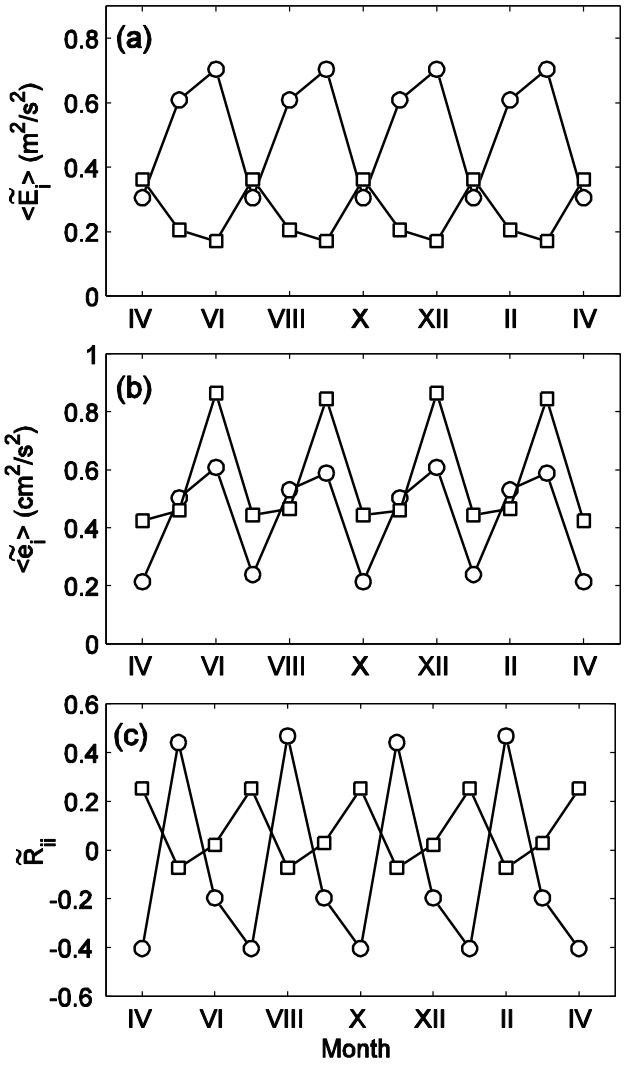


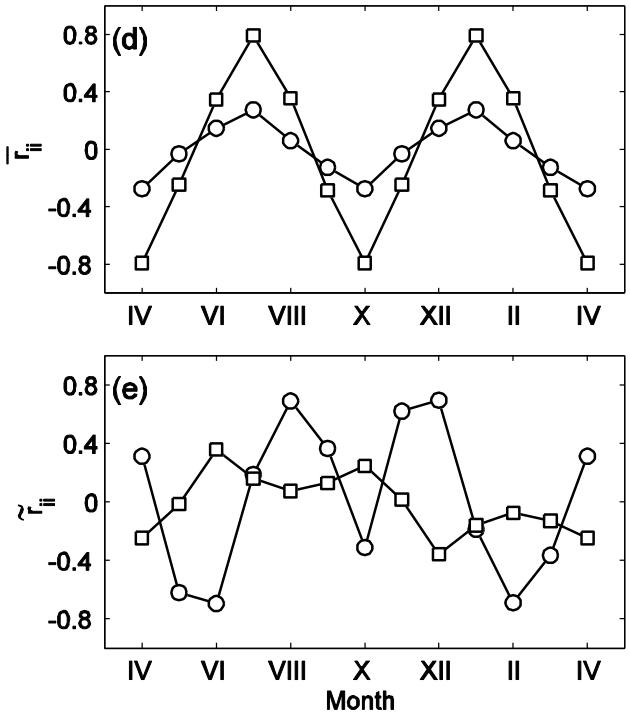




Semiannual Component in the Eastern Sub-Basin

(a) wind KE
(b) current KE
(c) corr wind stress and currents
(d) corr between semi-annual currents and mean wind
(e) corr between semiannual currents and annual wind stress





Results

- The annual and semi-annual unstable standing Rossby waves are detected in both the western and eastern sub-basins.

- The wind-driven Ekman pumping seems to be responsible for the standing wave generation in both the sub-basins.

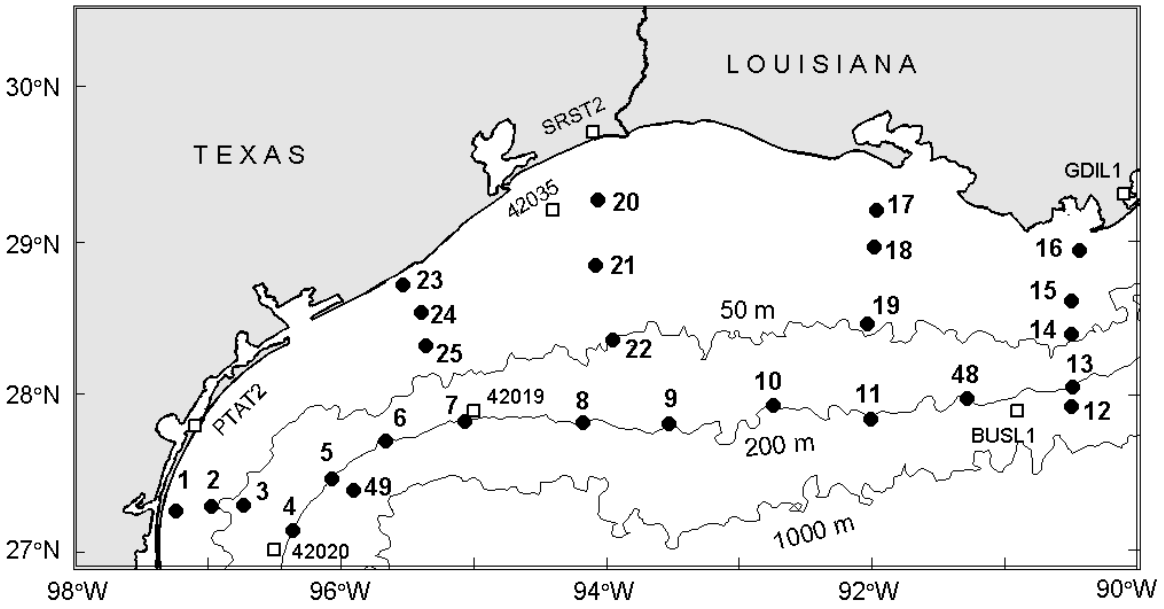
(b) Synoptic Current Reversals on the Texas-Louisiana Continental Shelf (Surface Drifting Buoys)

Ocean Velocity Observation

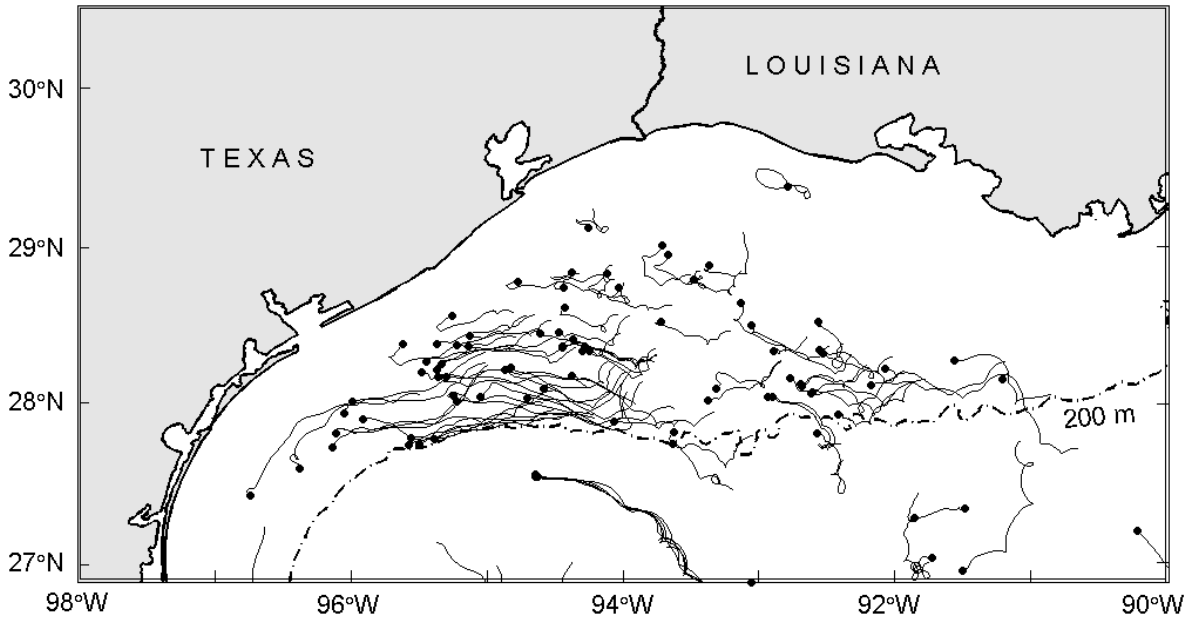
- 31 near-surface (10-14 m) current meter moorings during LATEX from April 1992 to November 1994

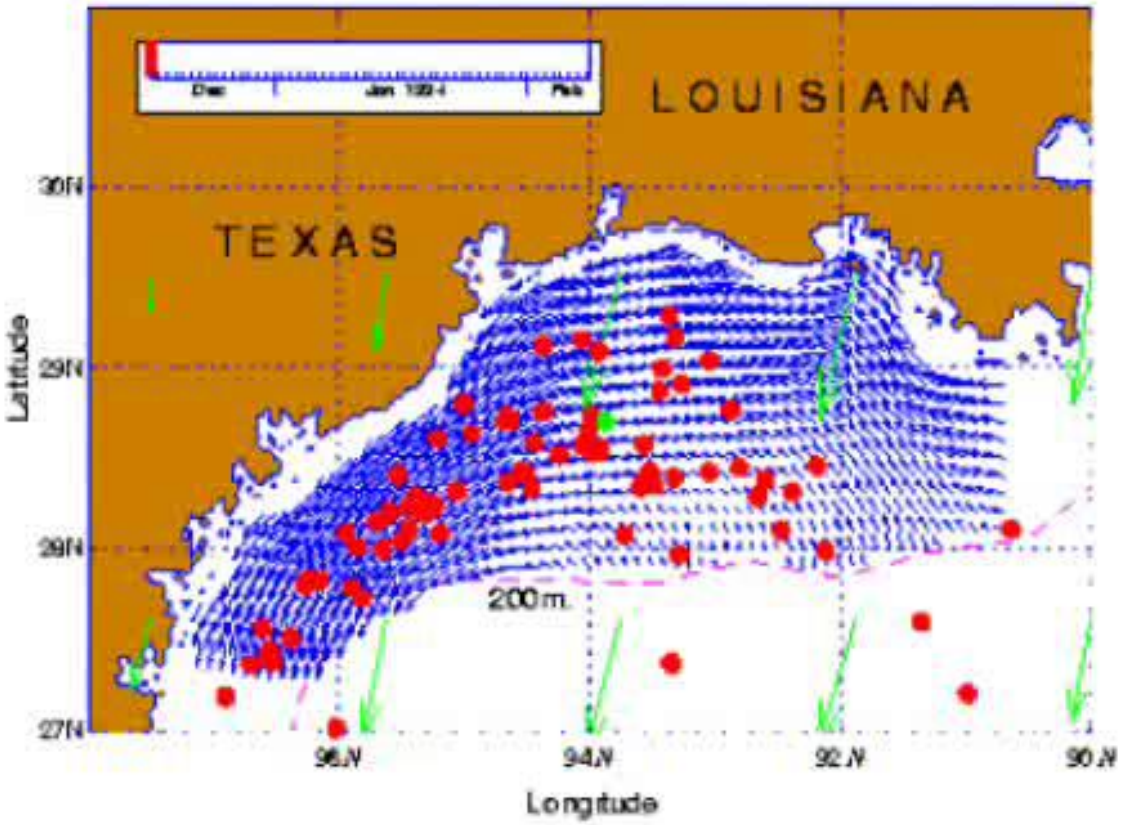
- Drifting buoys deployed at the first segment of the Surface Current and Lagrangian-drift Program (SCULP-I) from October 1993 to July 1994.

Moorings and Buoys



LTCS current reversal detected from SCULP-I drift trajectories.



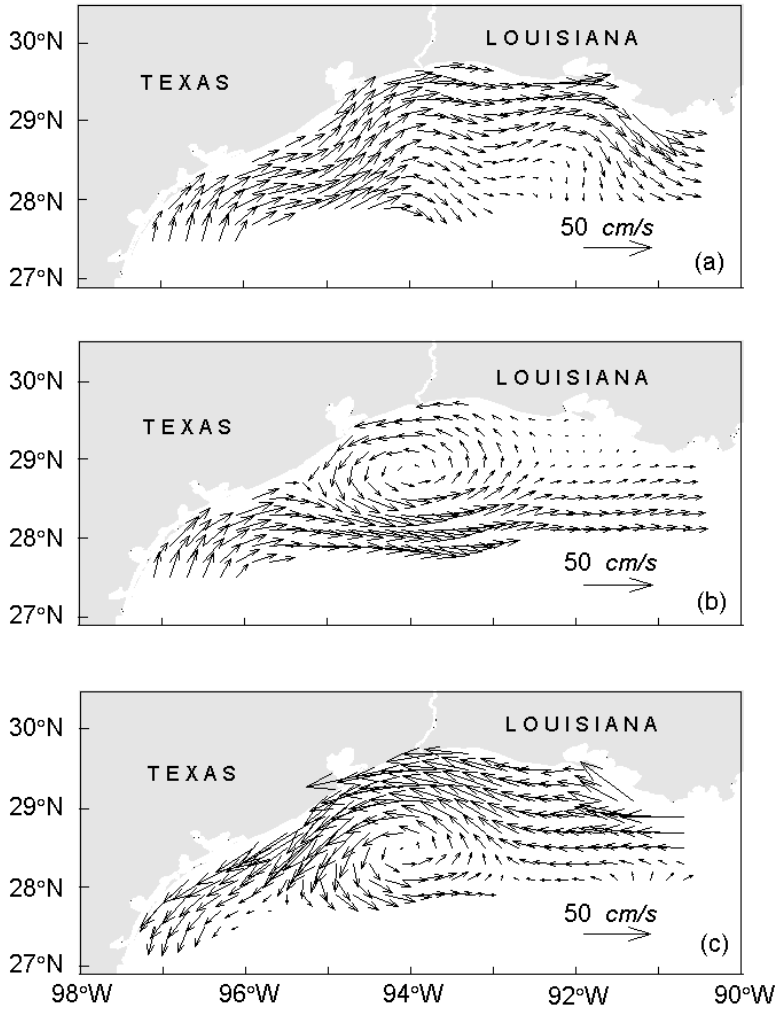

LOUISIANA
TEXAS
30N
29N
28N
27N
96N
94N
92N
90N
200m
Latitude
Longitude

LTCS current reversal detected from the reconstructed velocity data

December 30, 1993

January 3, 1994

January 6, 1994



EOF Analysis of the Reconstructed Velocity Filed

EOF	Variance (%)		
	01/21/93-05/21/93	12/19/93-04/17/94	10/05/94-11/29/94
1	80.2	77.1	74.4
2	10.1	9.5	9.3
3	3.9	5.6	6.9
4	1.4	3.3	4.6
5	1.1	1.4	2.3
6	0.7	1.1	0.8

Mean and First EOF Mode

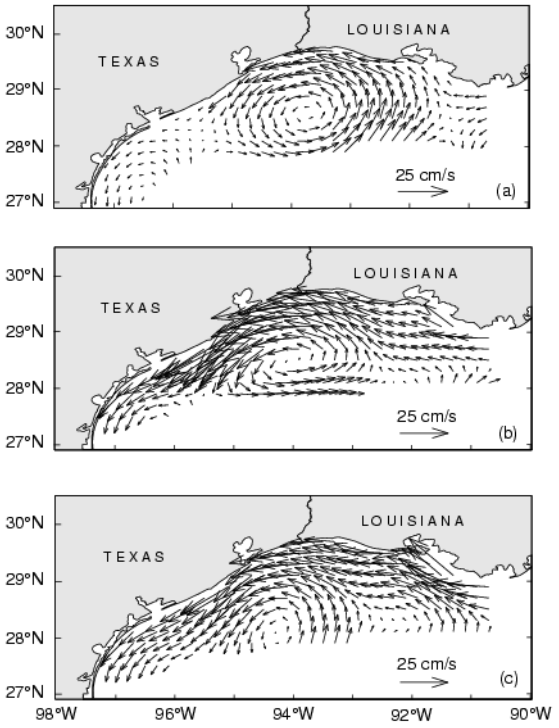
$$\tilde{\mathbf{u}}(x, y, t) = \overline{\mathbf{u}}(x, y) + A_1(t)\mathbf{u}_1(x, y),$$

Mean Circulation

1. First Period (01/21-05/21/93)

2. Second Period 12/19/93-04/17/94)

3. Third Period (10/05-11/29/94)

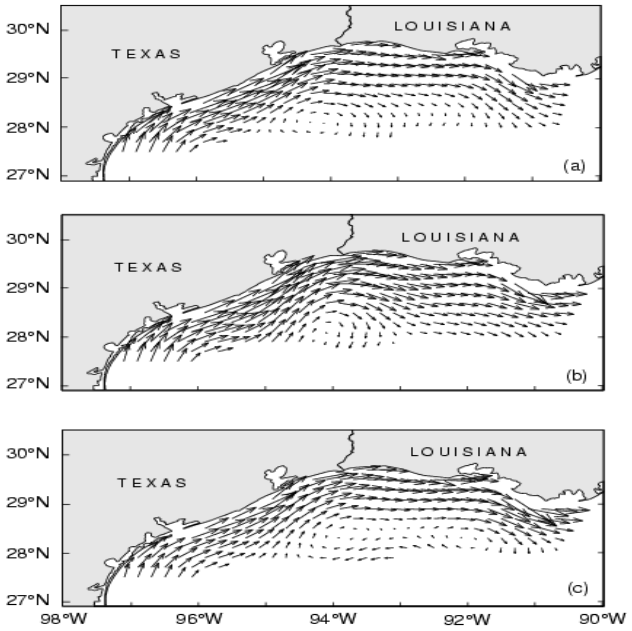


EOF1

1. First Period (01/21-05/21/93)

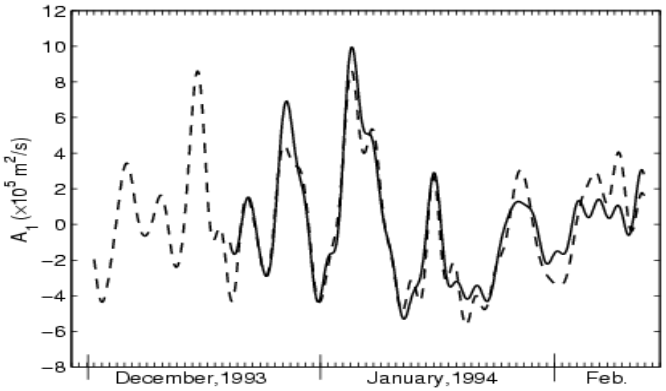
2. Second Period 12/19/93-04/17/94)

3. Third Period (10/05-11/29/94)



- Calculated $A_1(t)$

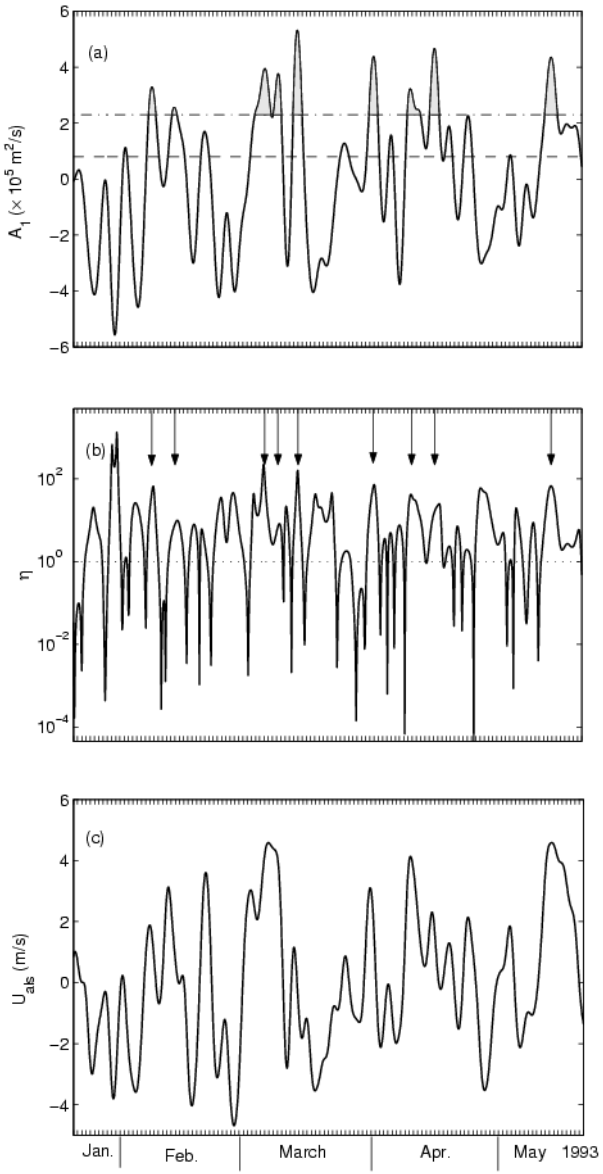
Using Current Meter Mooring (solid) and SCULP-1 Drifters (dashed)



- 8 total reversals observed

$$\eta = A_1^2 / \sum_{n=2}^{6} A_n^2$$

- U_{als} ~ alongshore wind

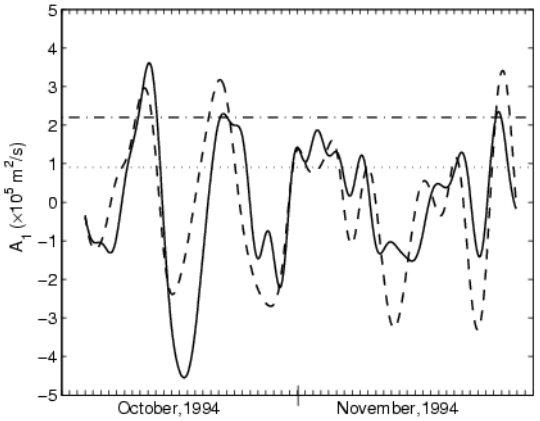


Surface Wind Data

- **7 buoys of the National Data Buoy Center (NDBC) and industry (C-MAN) around LATEX area**

- Regression between
- $A_1(t)$ and Surface
- Winds

- Solid Curve (reconstructed)
- Dashed Curve (predicted using winds)



$$A_1(t) = \alpha\left[U(t) - \overline{U}\right] + \beta\left[V(t) - \overline{V}\right] + \gamma$$

Results

- Alongshore wind forcing is the major factor causing the synoptic current reversal.

- Other factors, such as the Mississippi-Atchafalaya River discharge and offshore eddies of Loop Current origin, may affect the reversal threshold, but can not cause the synoptic current reversal.

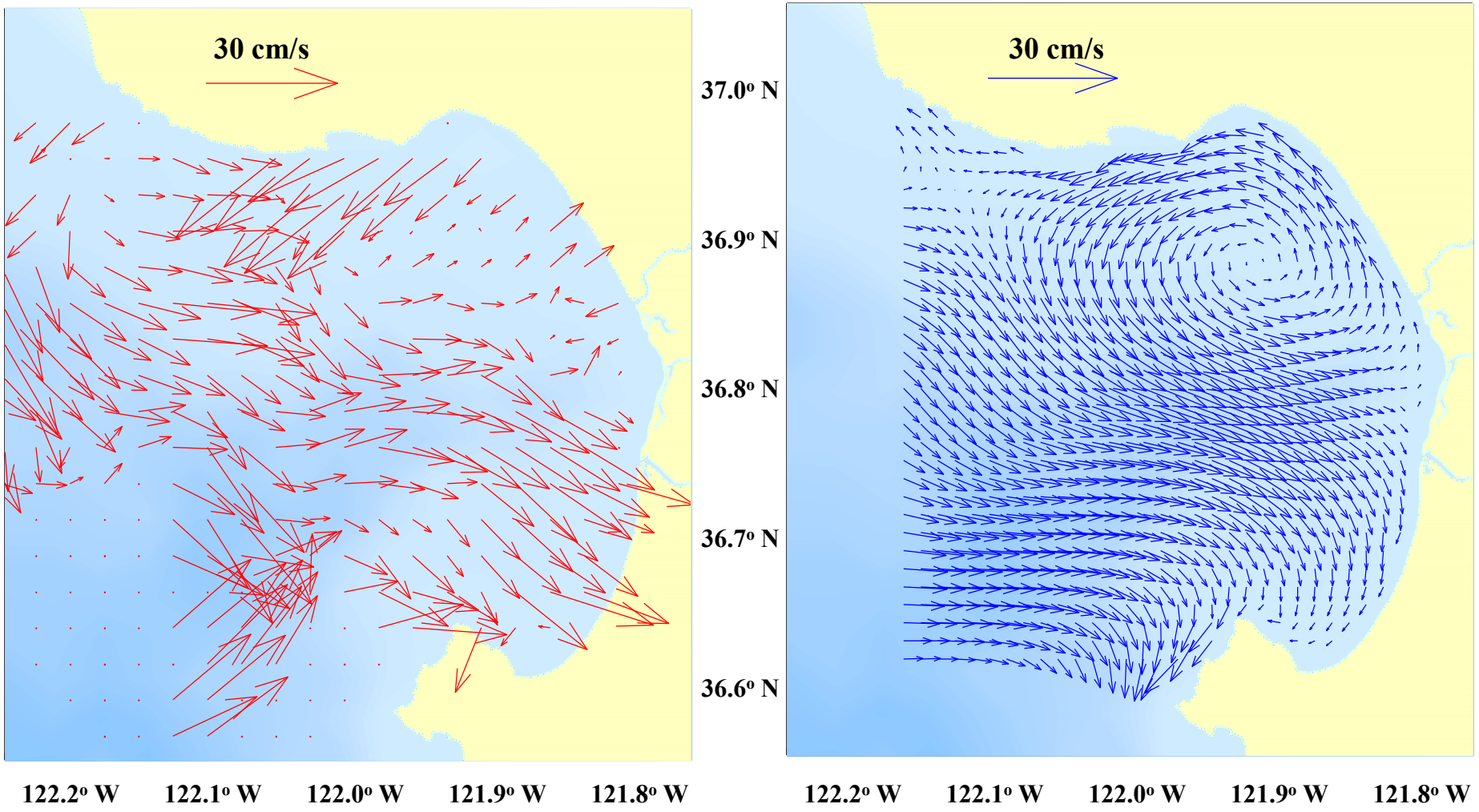
(c) Monterey Bay Surface Circulation (CODAR)

CODAR



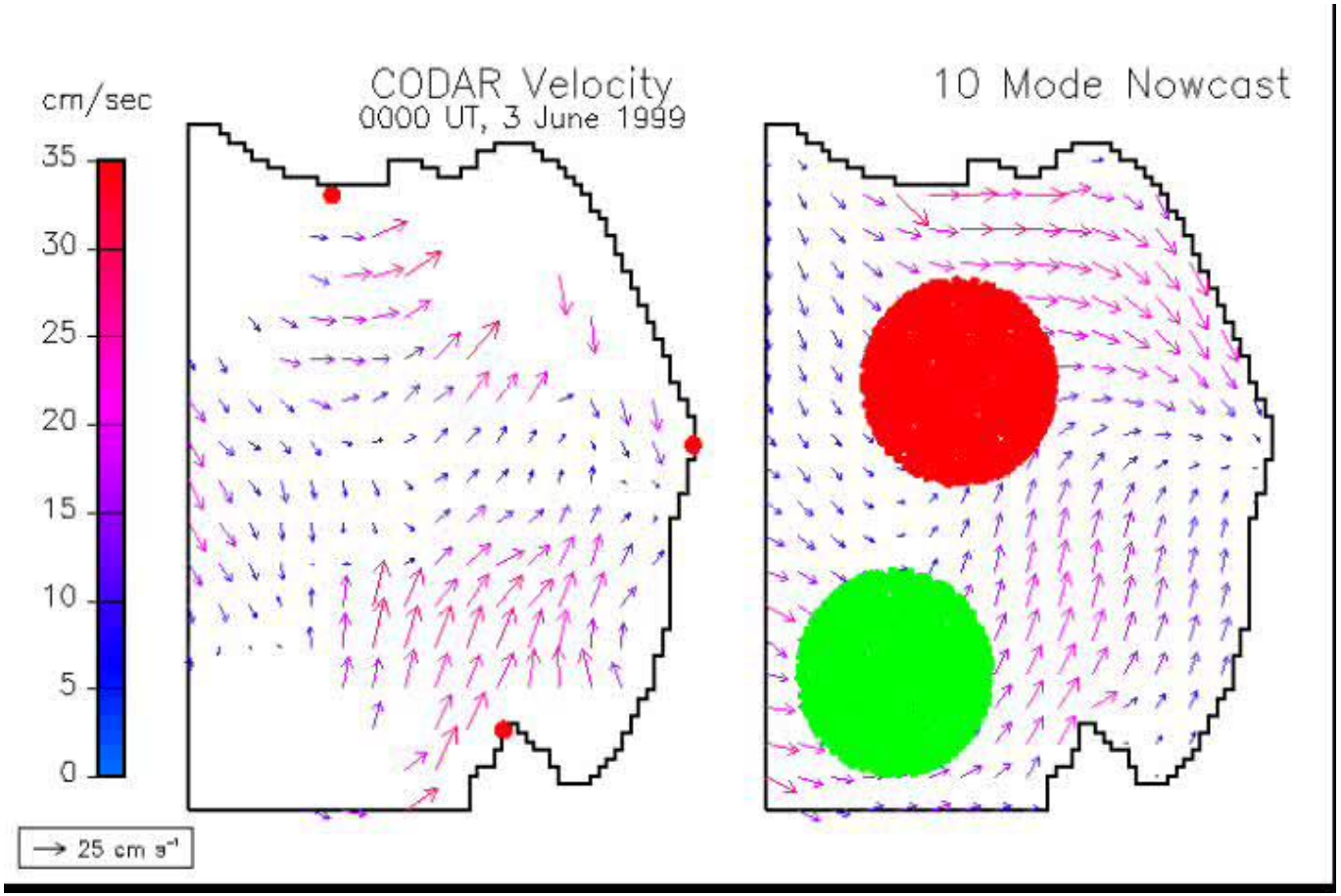
Monterey Bay





Place for comments: left - radar derived currents for 17:00 UT December 1, 1999

right – reconstructed velocity field.


cm/sec
35
30
25
20
15
10
5
0
CODAR Velocity
0000 UT, 3 June 1999
10 Mode Nowcast
→ 25 cm s⁻¹

Part-3
Modeling Application

Two Issues in Ocean Modeling

- How long is an ocean (or atmospheric) model valid once being integrated from its initial state?

- How can a numerical model be evaluated effectively?

References

- Chu, P.C., L.M. Ivanov, T. M. Margolina, and O.V. Melnichenko, On probabilistic stability of an atmospheric model to various amplitude perturbations. Journal of the Atmospheric Sciences, 59, 2860-2873.
- Chu, P.C., L.M. Ivanov, C.W. Fan, 2002: Backward Fokker-Planck equation for determining model valid prediction period. Journal of Geophysical Research, 107, C6, 10.1029/2001JC000879.
- Chu, P.C., L. Ivanov, L. Kantha, O. Melnichenko, and Y. Poberezhny, 2002: Power law decay in model predictability skill. Geophysical Research Letters, 29 (15), 10.1029/2002GLO14891.
- Chu, P.C., L.M. Ivanov, L.H. Kantha, T.M. Margolina, and O.M. Melnichenko, and Y.A, Poberenzhny, 2004: Lagrangian predictabilty of high-resolution regional ocean models. Nonlinear Processes in Geophysics, 11, 47-66.
- Chu, P.C., 2008: First passage time analysis on climate indices. Journal of Atmospheric and Oceanic Technology, 25, 258-270.
- Ivanov, L. M., and P.C. Chu, 2007a: On stochastic stability of regional ocean models with uncertainty in wind forcing. Nonlinear Processes in Geophysics, 14, 655-678.
- Ivanov, L. M., and P.C. Chu, 2007b: On stochastic stability of regional ocean models to finite-amplitude perturbations of initial conditions. Dynamics of Atmosphere and Oceans, 43 (3-4), 199-225..

(1) First-Passage Time

Physical Reality

- $\boldsymbol{Y}$
- Physical Law: $d\boldsymbol{Y}/dt = \boldsymbol{h}(\boldsymbol{y}, t)$
- Initial Condition: $\boldsymbol{Y}(t_0) = \boldsymbol{Y}_0$

Atmospheric & Oceanic Models

-
  - $\boldsymbol{X}$ is the prediction of **Y**
  - $d\boldsymbol{X}/dt = \boldsymbol{f}(\boldsymbol{X}, t) + q(t)\,\boldsymbol{X}$
  - Initial Condition: $\boldsymbol{X}(t_0) = \boldsymbol{X}_0$
  - Stochastic Forcing:
  - $\langle q(t) \rangle = 0$
  - $\langle q(t)q(t') \rangle = q^2\delta(t-t')$

Model Error

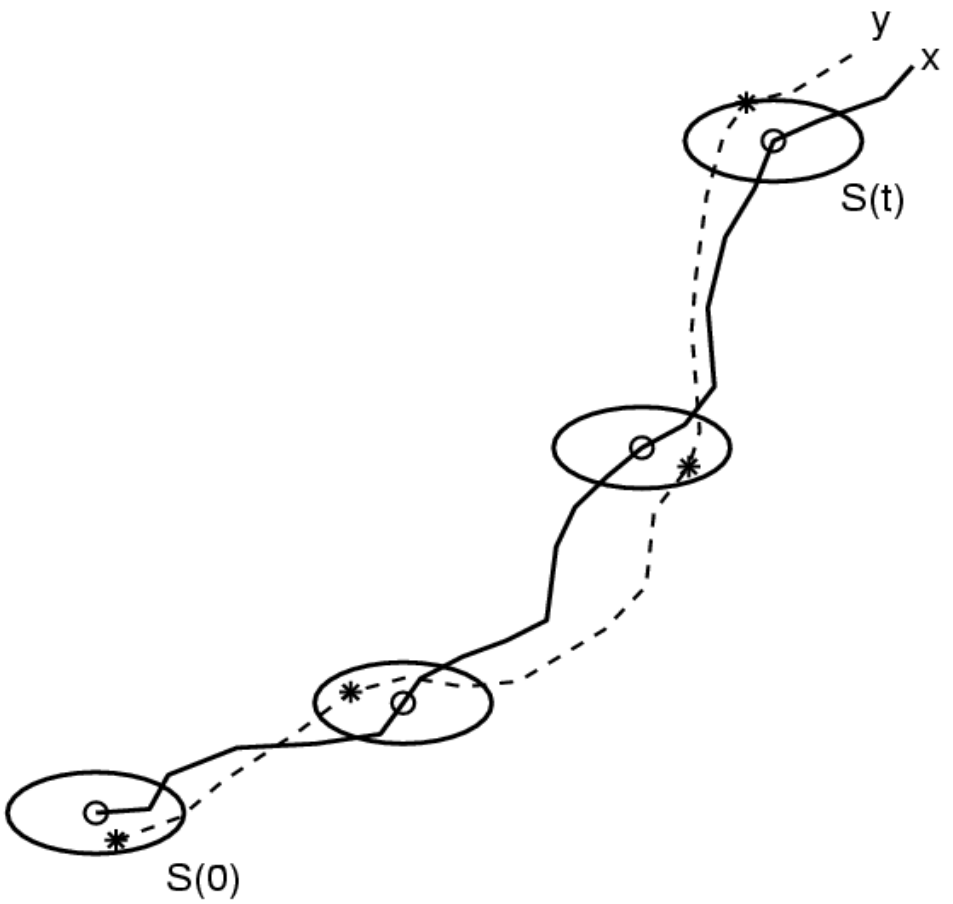
-
- $Z = X - Y$

- Initial*:* $Z_0 = X_0 - Y_0$

One Missing Parameter

- Tolerance Level ε
- Maximum accepted error

First Passage Time (FPT)

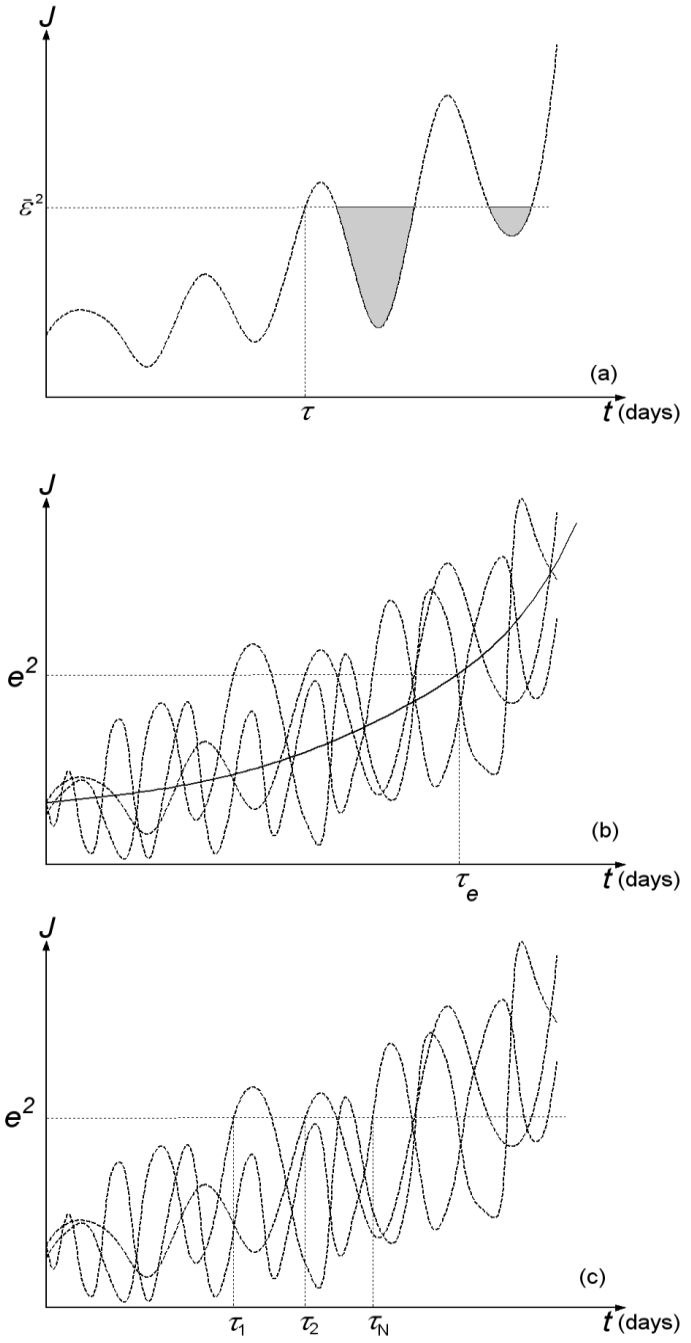


FPT is defined as the time period when the prediction error first exceeds a pre-determined criterion (i.e., the tolerance level ε).

First-Passage Time



The FPT and e-folding time for an oscillating prediction error: (a) FPT computed in an individual forecast. Shaded zones show returns of model predictability.
(b) an ensemble of (dashed curves), the ensemble averaged (solid curve) and the e-folding time, and
(c) the ensemble of (dashed curves) and appropriate ensemble of FPT.



Conditional Probability Density Function

- Initial Error: $\boldsymbol{z}_0$
- $(t - t_0)$? Random Variable
- Conditional PDF of $(t - t_0)$ with given $\boldsymbol{z}_0$?
  - $P[(t - t_0) | \boldsymbol{z}_0]$

Two Approaches

- Analytical (low dimension dynamical system)
- Practical (operational atmospheric or ocean model)

(2) Backward Fokker-Planck Equation

$$\frac{\partial P}{\partial t}-\sum_{i=1}^{J}\left(f_i-\frac{d\hat{x}_i}{dt}\right)\frac{\partial P}{\partial z_i^0}-\frac{1}{2}\sum_{i=1}^{J}\sum_{j=1}^{J}\sum_{l=1}^{J}k_{il}k_{lj}\frac{\partial^2 P}{\partial z_i^0\partial z_j^0}=0,$$

Moments

$$\tau_1(\mathbf{z}_0) = \int_{t_0}^{\infty} P(t_0, \mathbf{z}_0, t - t_0)(t - t_0)dt$$

$$\tau_2(\mathbf{z}_0) = \int_{t_0}^{\infty} P(t_0, \mathbf{z}_0, t - t_0)(t - t_0)^2 dt$$

Example-1: Maximum Growing Maniford of Lorenz System (Nicolis, 1992)

- $$\frac{d\xi}{dt} = (\sigma - g\xi^2) + v(t)\xi, \qquad 0 \le \xi < \infty$$

$$\langle v(t) \rangle = 0, \qquad \langle v(t)v(t') \rangle = q^2 \delta(t - t').$$

$$\sigma = 0.64, \qquad g = 0.3, \qquad q^2 = 0.2.$$

Mean and Variance of FPT

$$(\sigma\xi_0 - g\xi_0^2)\frac{d\tau_1}{d\xi_0} + \frac{q^2\xi_0^2}{2}\frac{d^2\tau_1}{d\xi_0^2} = -1$$

$$(\sigma\xi_0 - g\xi_0^2)\frac{d\tau_2}{d\xi_0} + \frac{q^2\xi_0^2}{2}\frac{d^2\tau_2}{d\xi_0^2} = -2\tau_1$$

$\tau_1 = 0, \quad \tau_2 = 0$ for $\xi_0 = \varepsilon$.

$\frac{d\tau_1}{d\xi_0} = 0, \quad \frac{d\tau_2}{d\xi_0} = 0$ for $\xi_0 = \xi_{noise}$.

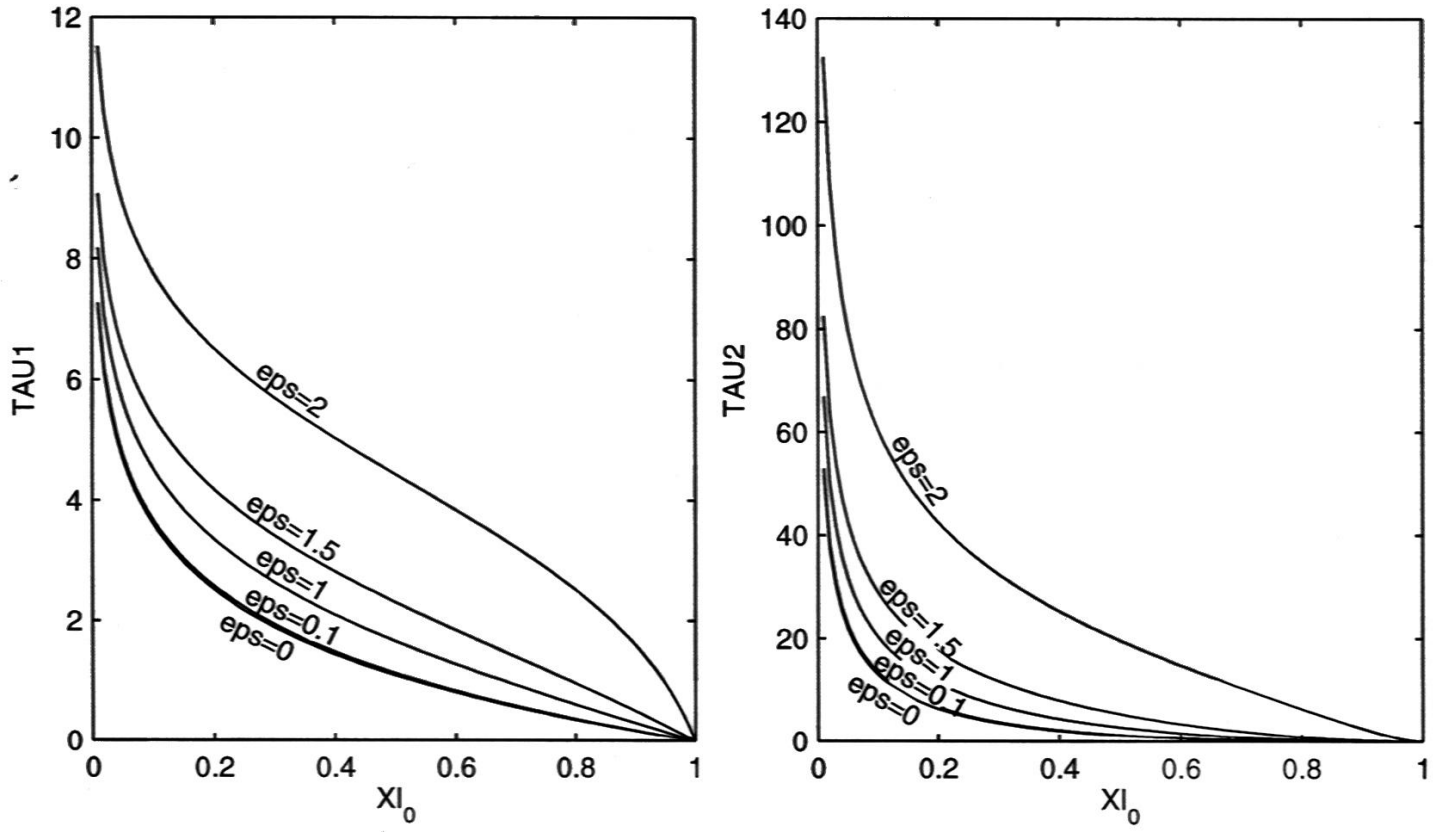
Analytical Solutions

$$\tau_1(\bar{\xi}_0, \bar{\xi}_{noise}, \varepsilon) = \frac{2}{q^2} \int_{\bar{\xi}_0}^{1} y^{-\frac{2\sigma}{q^2}} \exp\left(\frac{2\varepsilon g}{q^2} y\right) \left[\int_{\bar{\xi}_{noise}}^{y} x^{\frac{2\sigma}{q^2}-2} \exp\left(-\frac{2\varepsilon g}{q^2} x\right) dx \right] dy$$

$$\tau_2(\bar{\xi}_0, \bar{\xi}_{noise}, \varepsilon) = \frac{4}{q^2} \int_{\bar{\xi}_0}^{1} y^{-\frac{2\sigma}{q^2}} \exp\left(\frac{2\varepsilon g}{q^2} y\right) \left[\int_{\bar{\xi}_{noise}}^{y} \tau_1(x) x^{\frac{2\sigma}{q^2}-2} \exp\left(-\frac{2\varepsilon g}{q^2} x\right) dx \right] dy$$

$$\bar{\xi}_0 = \xi_0 / \varepsilon, \qquad \bar{\xi}_{noise} = \xi_{noise} / \varepsilon$$

Dependence of tau1 & tau2 on Initial Condition Error (ξ_0/ε)



Example-2: Lorenz System (1984) Modified Hadley Circulation

$$\frac{dx_1}{dt} = -x_2^2 - x_3^2 - ax_1 + aF,$$

$$\frac{dx_2}{dt} = x_1 x_2 - bx_1 x_3 - x_2 + G,$$

$$\frac{dx_3}{dt} = bx_1 x_2 + x_1 x_3 - x_3,$$

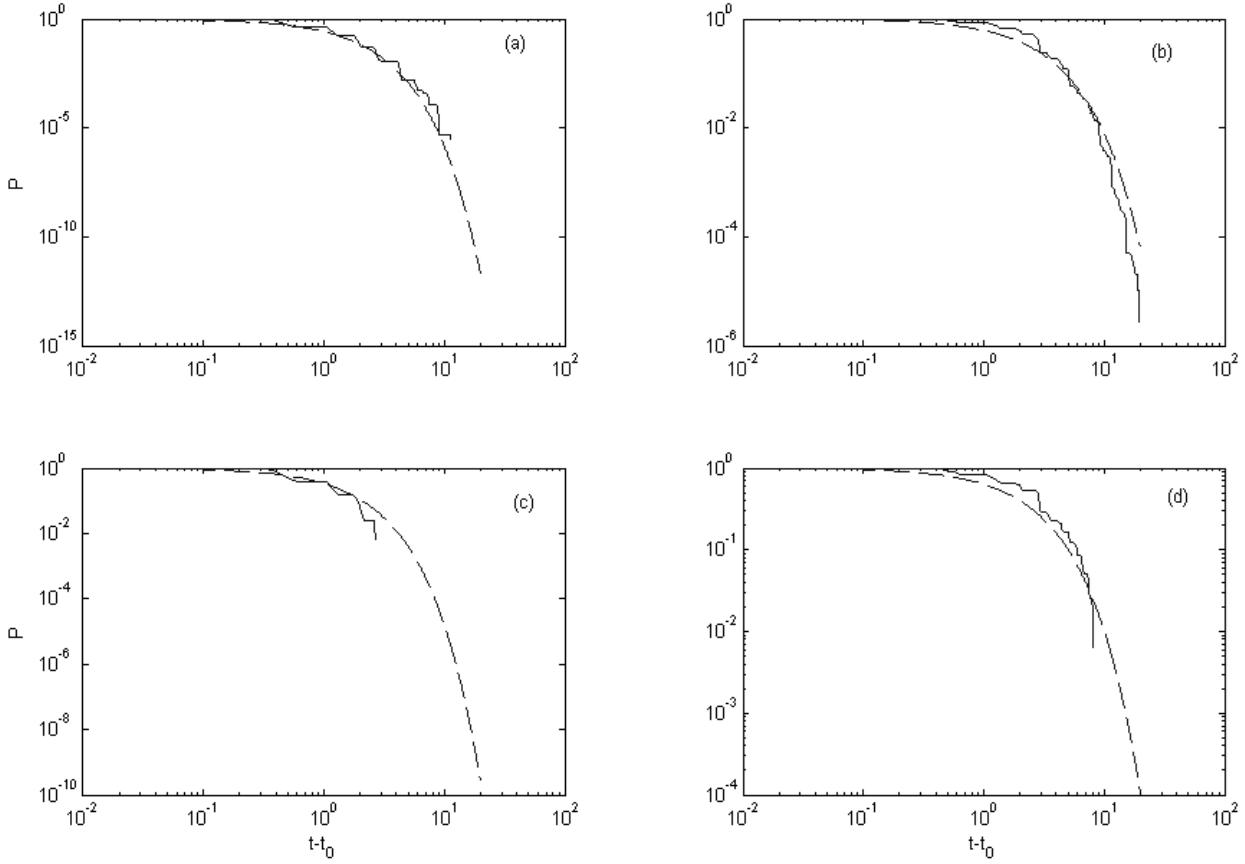
Sensitivity of PDF on the tolerance level and ensemble dimension: numerical (solid curve), analytic (dashed curve)

ε=0.1

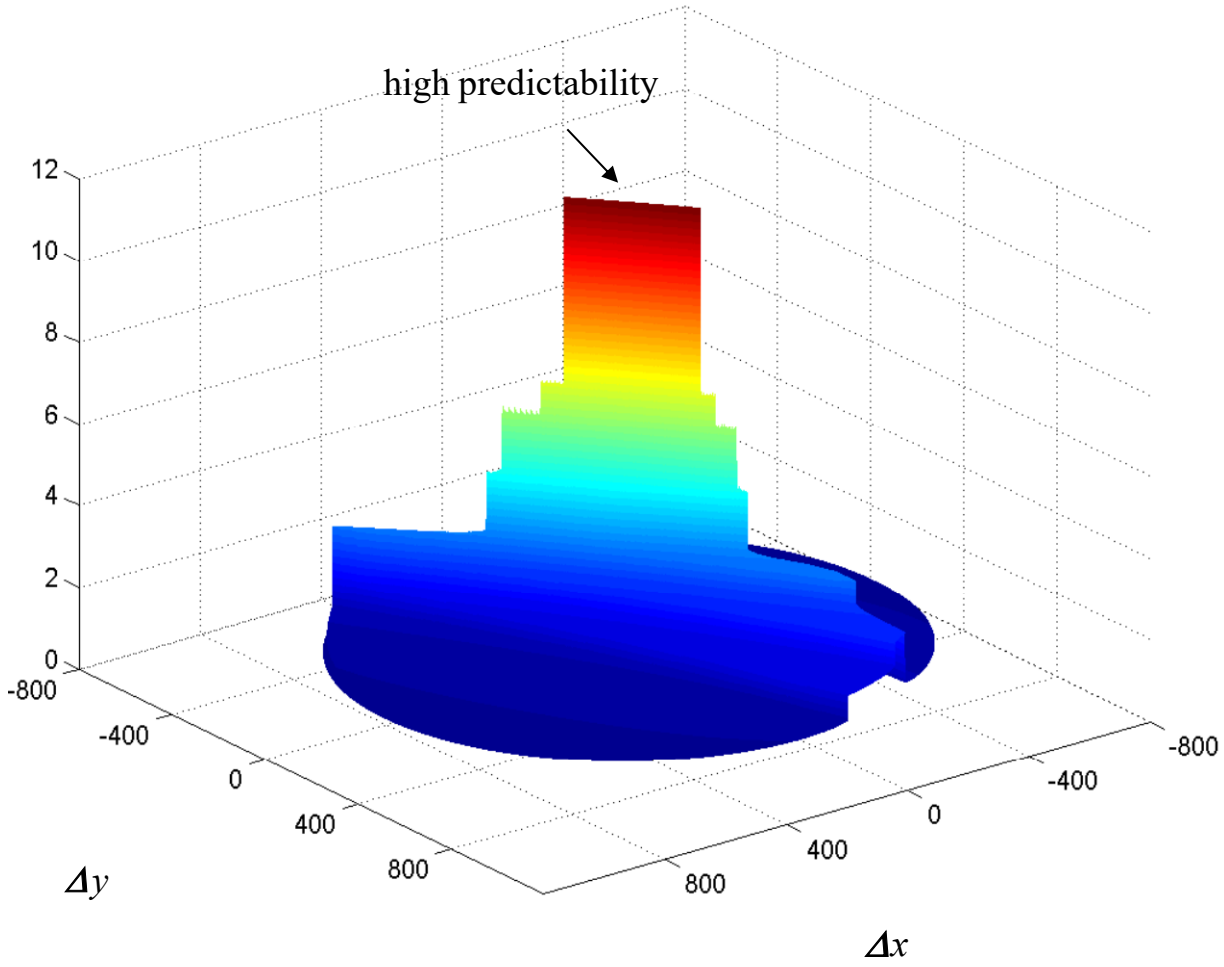
ε=0.5

N=250,000

N=100



Dependence of FPT on Initial Error (Dx, Dy) for $\varepsilon = 0.1$



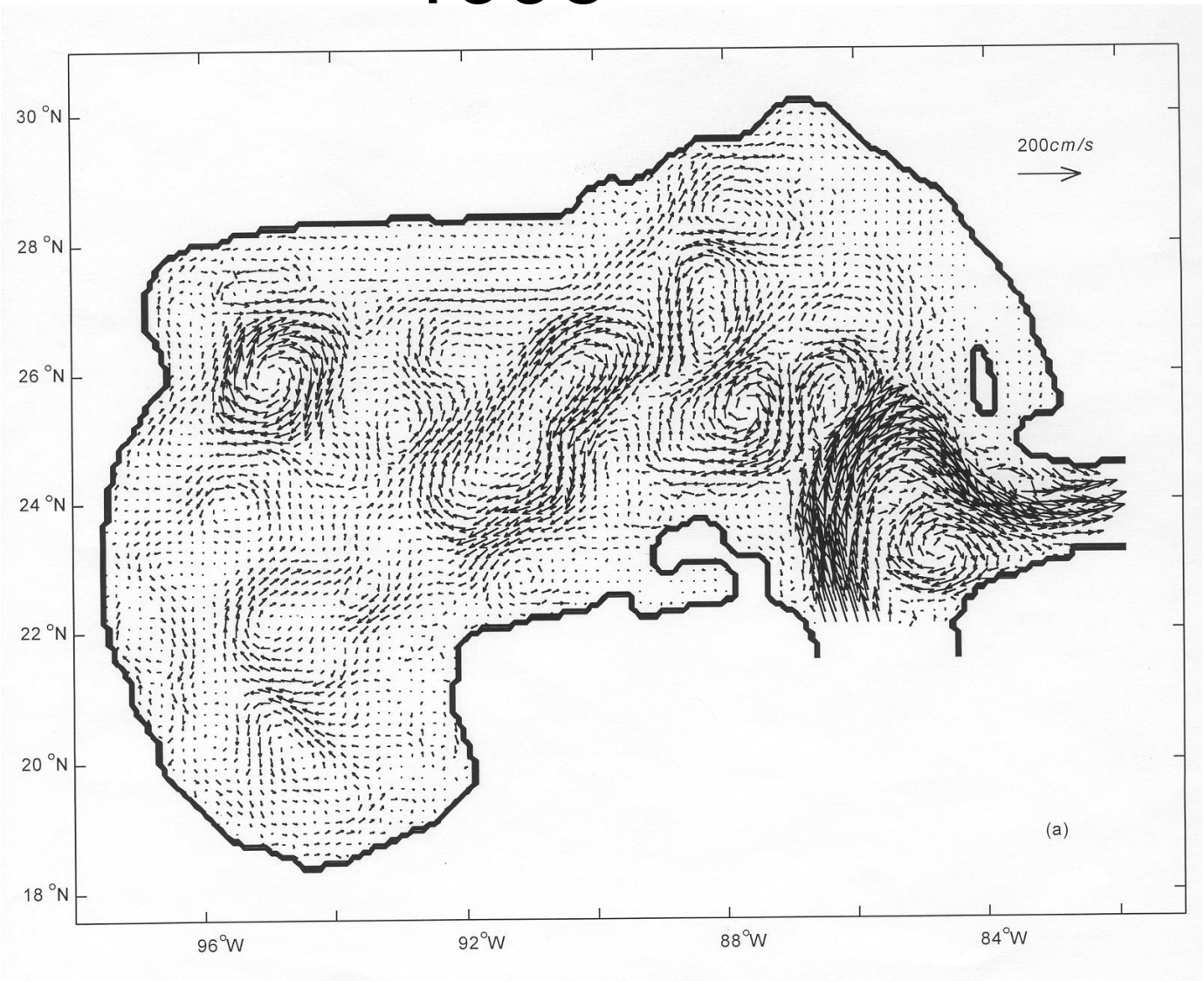
(3) Power Law Decay of Model Predictability Skill

Gulf of Mexico Prediction System

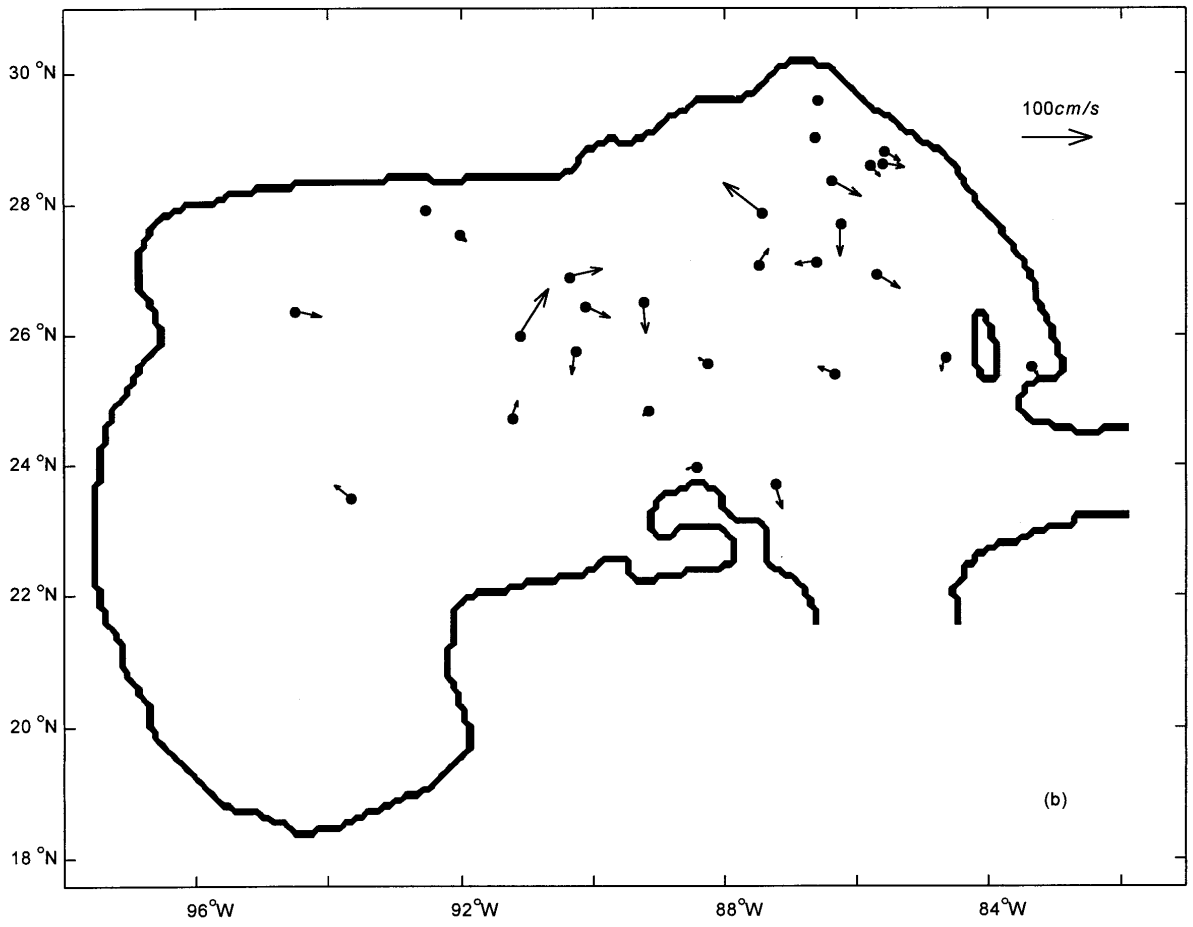
Gulf of Mexico Forecast System

- University of Colorado Version of POM
- 1/12^{o} Resolution
- Real-Time SSH Data (TOPEX, ESA ERS-1/2) Assimilated
- Real Time SST Data (MCSST, NOAA AVHRR) Assimilated
- Six Months Four-Times Daily Data From July 9, 1998 for Verification

Model Generated Velocity Vectors at 50 m on 00:00 July 9, 1998



(Observational) Drifter Data at 50 m on 00:00 July 9, 1998



Error Mean and Variance

Error Mean $$L_1 = \langle \mathbf{z} \rangle$$

Error Variance $$L_2 = \left\langle \left(\mathbf{z} - \langle \mathbf{z} \rangle\right)^t \left(\mathbf{z} - \langle \mathbf{z} \rangle\right) \right\rangle$$

Exponential Error Growth

$$L_1 \propto e^{\sigma t}, \qquad L_2 \propto e^{\omega t},$$

Classical Linear Theory

No Long-Term Predictability

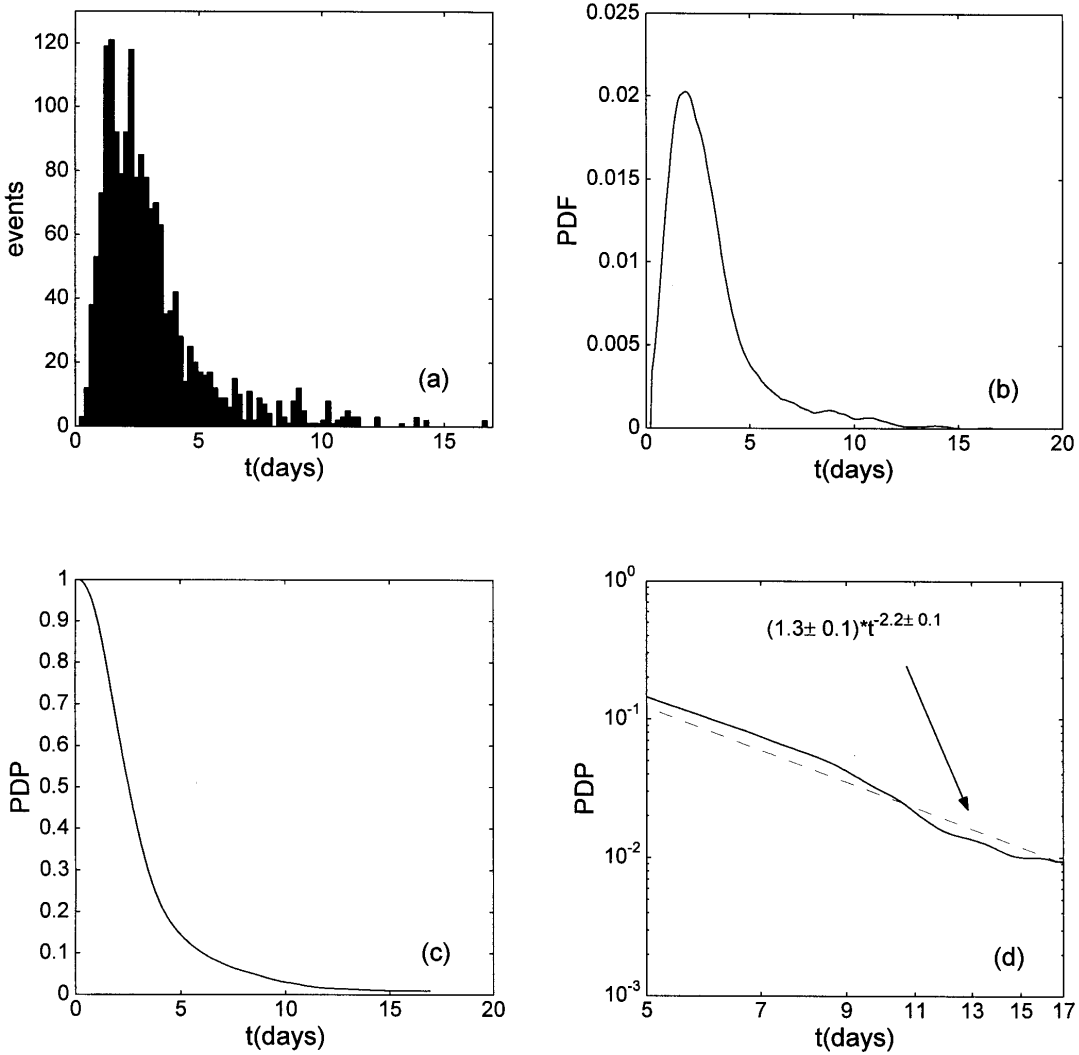
Power Law

$$L_1 \propto t^{\alpha}, \qquad L_2 \propto t^{\beta},$$

$$P(t_0, \mathbf{z}_0, \varepsilon, t - t_0) \sim t^{-\gamma} \quad \text{for large } t.$$

Long-Term Predictability May Occur

Statistical Characteristics of VPP for zero initial error and 22 km tolerance level (Non-Gaussion)

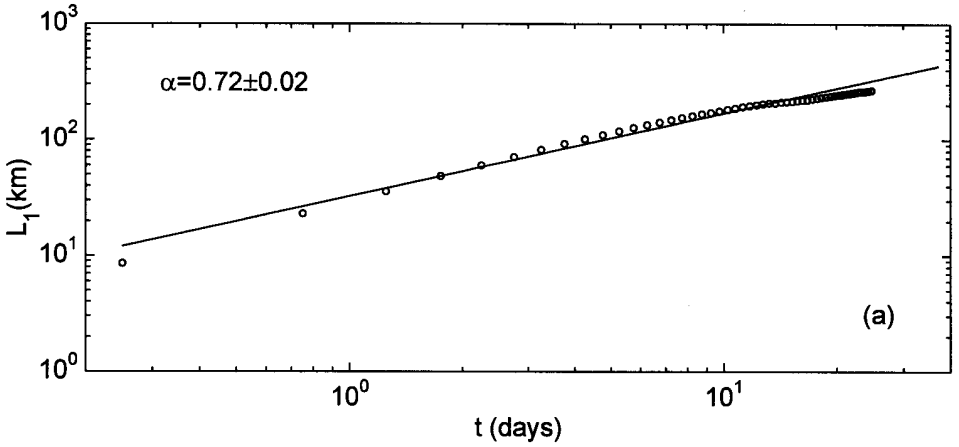


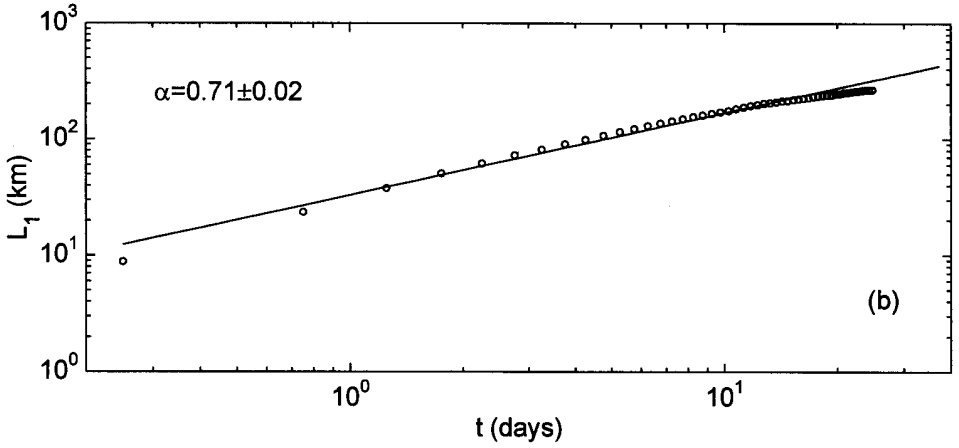
Scaling behavior of the mean error (L_1) growth for initial error levels:

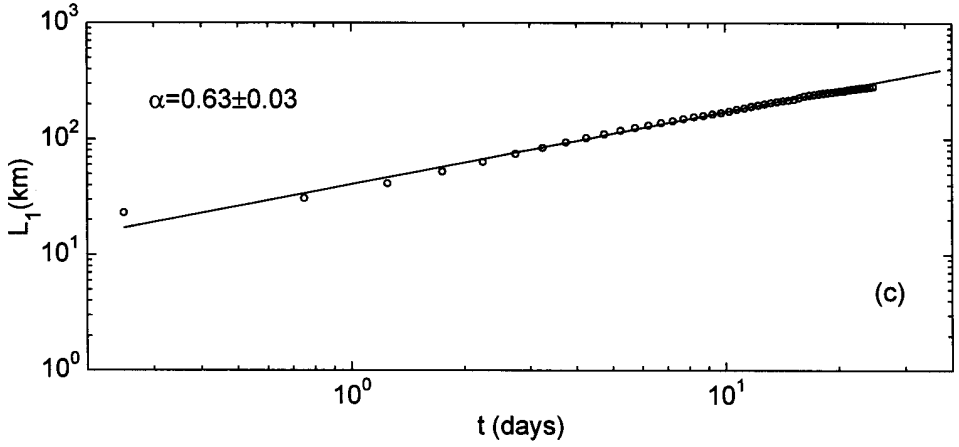
(a) 0

(b) 2.2 km

(c) 22 km







Scaling behavior of the

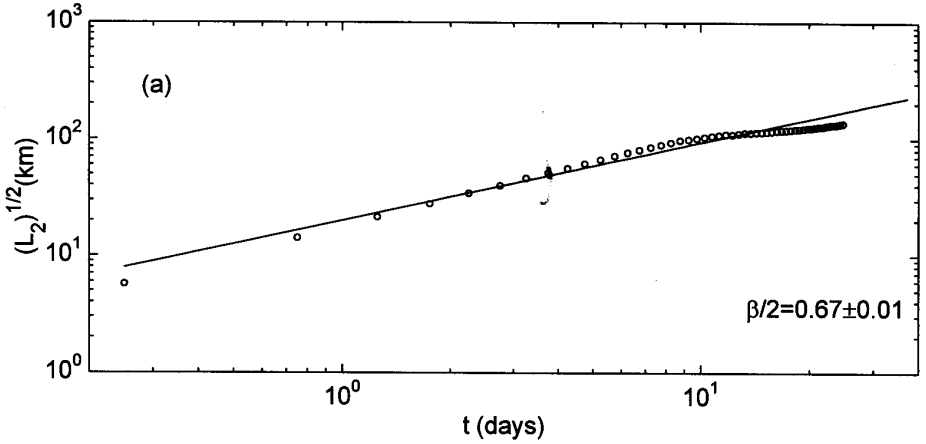
Error variance (L_2) growth

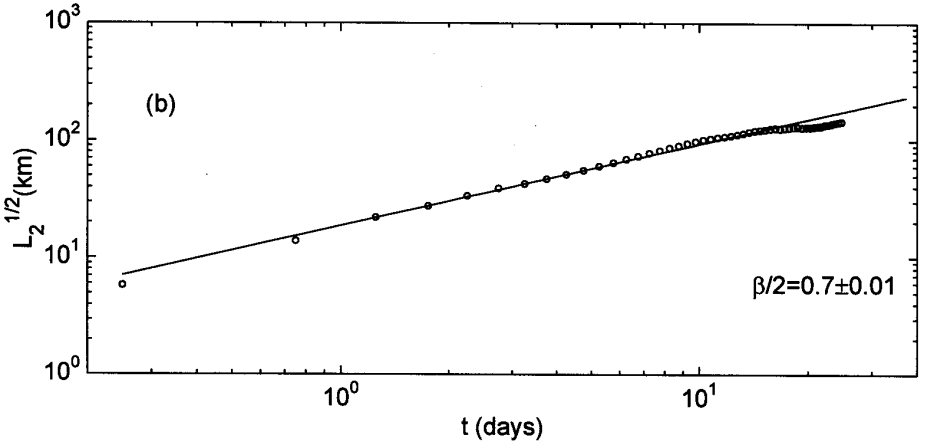
for initial error levels:

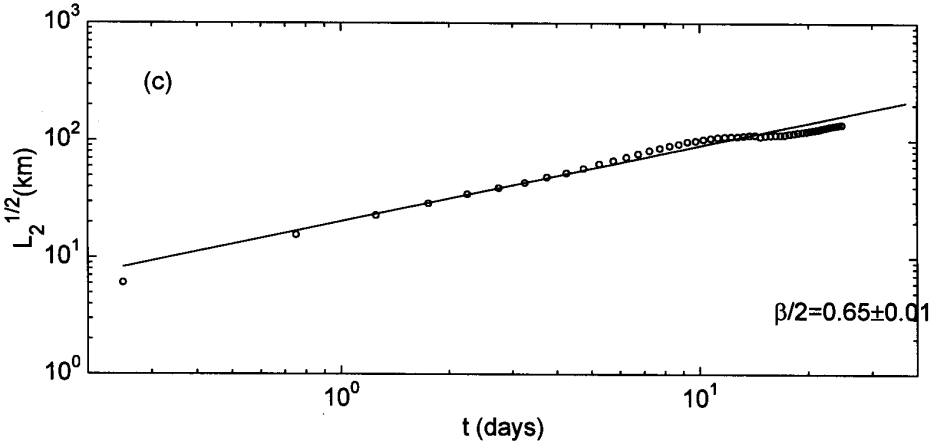
(a) 0

(b) 2.2 km

(c) 22 km

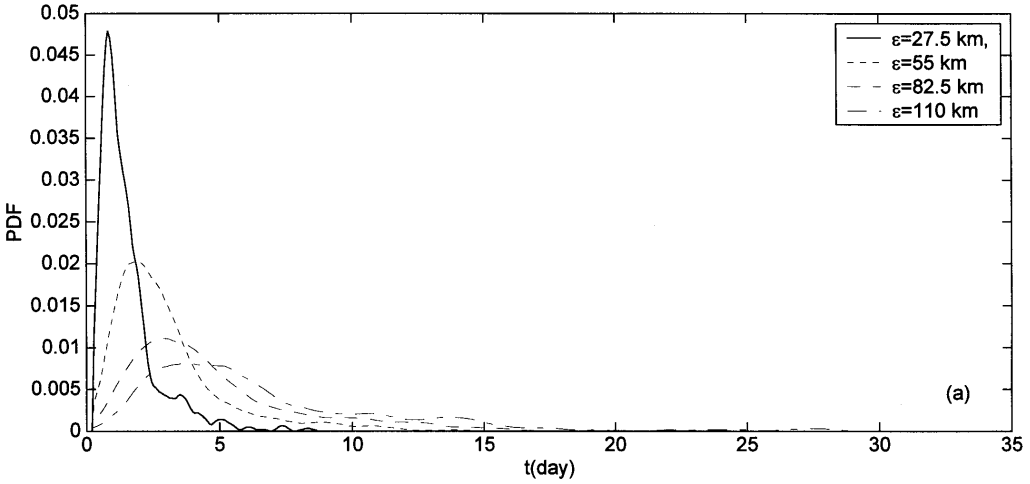


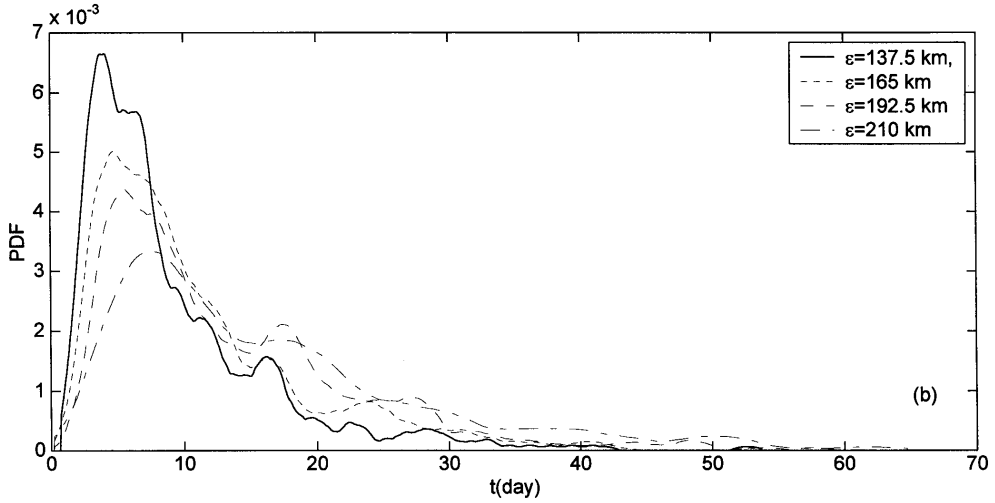




Probability Density Function of VPP calculated with different tolerance levels

Non-Gaussian distribution with long tail toward large values of VPP (Long-term Predictability)





The FPT analysis is usually conducted in the phase space.

Predictability Tube

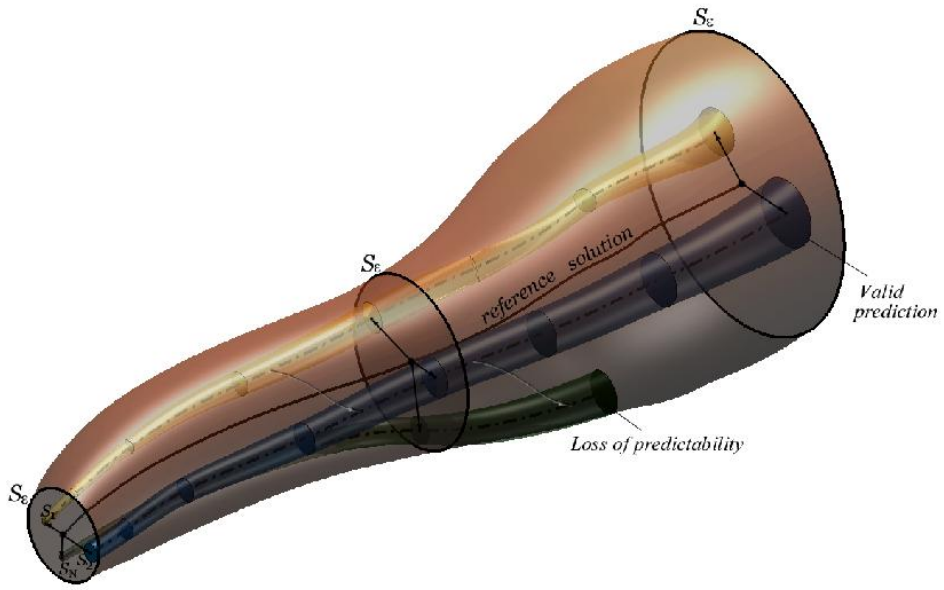


Fig. 31

Conclusions

- OSD is a useful tool for processing real-time velocity data with short duration and limited-area sampling.
- The scheme can handle highly noisy data.
- The scheme is model independent.
- The scheme can be used for velocity data assimilation.
- Phase Space Consideration